



Terrestrial or marine – indications towards the origin of ice-nucleating particles during melt season in the European Arctic up to 83.7° N

Markus Hartmann¹, Xianda Gong^{1,c}, Simonas Kecorius¹, Manuela van Pinxteren², Teresa Vogl^{1,a}, André Welti^{1,b}, Heike Wex¹, Sebastian Zeppenfeld², Hartmut Herrmann², Alfred Wiedensohler¹, and Frank Stratmann¹

¹Experimental Aerosol and Cloud Microphysics, Leibniz Institute for Tropospheric Research, 04318, Leipzig, Germany

²Atmospheric Chemistry, Leibniz Institute for Tropospheric Research, 04318, Leipzig, Germany

^anow at: Remote Sensing and The Arctic Climate System, Leipzig Institute for Meteorology, University of Leipzig, 04103, Leipzig, Germany

^bnow at: Finnish Meteorological Institute, Helsinki, Finland

^cnow at: Center for Aerosol Science and Engineering, Department of Energy, Environmental and Chemical Engineering, Washington University in St. Louis, St. Louis, USA

Correspondence: Markus Hartmann (markus.hartmann@tropos.de)

Received: 24 November 2020 – Discussion started: 26 November 2020

Revised: 27 May 2021 – Accepted: 27 May 2021 – Published: 4 August 2021

Abstract. Ice-nucleating particles (INPs) initiate the primary ice formation in clouds at temperatures above ca. -38°C and have an impact on precipitation formation, cloud optical properties, and cloud persistence. Despite their roles in both weather and climate, INPs are not well characterized, especially in remote regions such as the Arctic. We present results from a ship-based campaign to the European Arctic during May to July 2017. We deployed a filter sampler and a continuous-flow diffusion chamber for offline and online INP analyses, respectively. We also investigated the ice nucleation properties of samples from different environmental compartments, i.e., the sea surface microlayer (SML), the bulk seawater (BSW), and fog water. Concentrations of INPs (N_{INP}) in the air vary between 2 to 3 orders of magnitudes at any particular temperature and are, except for the temperatures above -10°C and below -32°C , lower than in midlatitudes. In these temperature ranges, INP concentrations are the same or even higher than in the midlatitudes. By heating of the filter samples to 95°C for 1 h, we found a significant reduction in ice nucleation activity, i.e., indications that the INPs active at warmer temperatures are biogenic. At colder temperatures the INP population was likely dominated by mineral dust. The SML was found to be enriched in INPs compared to the BSW in almost all samples. The

enrichment factor (EF) varied mostly between 1 and 10, but EFs as high as 94.97 were also observed. Filtration of the seawater samples with $0.2\ \mu\text{m}$ syringe filters led to a significant reduction in ice activity, indicating the INPs are larger and/or are associated with particles larger than $0.2\ \mu\text{m}$. A closure study showed that aerosolization of SML and/or seawater alone cannot explain the observed airborne N_{INP} unless significant enrichment of INP by a factor of 10^5 takes place during the transfer from the ocean surface to the atmosphere. In the fog water samples with -3.47°C , we observed the highest freezing onset of any sample. A closure study connecting N_{INP} in fog water and the ambient N_{INP} derived from the filter samples shows good agreement of the concentrations in both compartments, which indicates that INPs in the air are likely all activated into fog droplets during fog events. In a case study, we considered a situation during which the ship was located in the marginal sea ice zone and N_{INP} levels in air and the SML were highest in the temperature range above -10°C . Chlorophyll *a* measurements by satellite remote sensing point towards the waters in the investigated region being biologically active. Similar slopes in the temperature spectra suggested a connection between the INP populations in the SML and the air. Air mass history had no influence on the observed airborne INP population. Therefore, we

conclude that during the case study collected airborne INPs originated from a local biogenic probably marine source.

1 Introduction

The Arctic is more sensitive to climate change than any other region on Earth, and changes are proceeding at an unprecedented pace and intensity (Serreze and Barry, 2011). The increase of the Arctic surface air temperature, the most prominent variable to indicate Arctic change, exceeds the warming in midlatitudes by about 2 K (Wendisch et al., 2017; Overland et al., 2011; Serreze and Barry, 2011). This enhanced warming phenomenon is referred to as Arctic amplification (AA). Arctic peculiarities together with multiple feedback mechanisms are known to contribute to the enhanced sensitivity of the Arctic (Wendisch et al., 2017). And, while the individual processes are known, the relative contribution of each process, their strengths, and the interlinkage leading to AA are still a field of ongoing research (Serreze and Barry, 2011; Pithan and Mauritsen, 2014; Cohen et al., 2020; Wendisch et al., 2017).

Aerosol particles are a key factor in cloud formation and can alter the microphysical properties of clouds (Pruppacher and Klett, 2010). The formation of clouds is further promoted by the increase in near-surface water vapor concentration due to the extended open water areas. Clouds and their properties are essential for the energy budget of the Arctic boundary layer. Arctic clouds are often at low levels, and they tend to warm the surface below the clouds (Intrieri, 2002; Shupe and Intrieri, 2004) and consequently cause more sea ice to melt (Vavrus et al., 2011). An increased cloud cover as well as the accompanying downward longwave radiation also prevents new sea ice from growing again, reducing the sea ice cover in the following seasons (Liu and Key, 2014; Park et al., 2015).

The visible manifestation of the Arctic climate change is the perennial sea ice cover decline, which has intensified over the last decade (Lang et al., 2017; Kwok et al., 2009). The decline in sea ice results in an overall increase in marine biological activity, which may give rise to new sources for aerosol particles and/or alter existing ones (Arrigo et al., 2008). Equivalently to the marine environment, the thawing of permafrost increases the terrestrial biological activity (Hinzman et al., 2005) and presumably the emission of primary aerosol particles and/or particle precursors (Creamean et al., 2020).

A number of studies showed that mixed-phase clouds prevail, existing in the temperature range between 0 and -38°C , in the Arctic (e.g., Intrieri, 2002; Pinto, 1998; Shupe et al., 2006, 2011; Turner, 2005). These clouds, which are composed of a mixture of supercooled droplets and ice crystals, typically extend over large areas and display extraordinary longevity despite their microphysically unstable nature. These clouds show a lower degree of glaciation in compari-

son to clouds at similar altitudes in other parts of the globe (Costa et al., 2017), which might be due to a lack of ice-nucleating particles (INPs). INPs are the catalyst needed for the primary ice formation at temperatures relevant for mixed-phase clouds and are thus essential to induce the freezing of supercooled liquid cloud droplets.

As INPs can directly affect the phase state of the cloud, their abundance and efficiency to initiate freezing also affects precipitation, lifetime, and the radiative effects of clouds (e.g., Loewe et al., 2017; Prenni et al., 2007; Ovchinnikov et al., 2014; Solomon et al., 2015). Solomon et al. (2018) even state that the influences of INPs regarding the radiative properties of Arctic clouds are more important than those of cloud condensation nuclei (CCN). This underlines the importance of gaining quantitative knowledge about the abundance, properties, nature, and sources of Arctic INPs.

Several previous studies have reported that marine as well as terrestrial sources contribute to Arctic INPs ice active at temperatures above approximately -15°C . For the marine environment, it was found that especially the sea surface microlayer (SML) can be highly ice active (Alpert et al., 2011a, b; Bigg, 1996; Bigg and Leck, 2008; Irish et al., 2017, 2019b; Knopf et al., 2011; Leck and Bigg, 2005; Schnell and Vali, 1976; Wilson et al., 2015; Zeppenfeld et al., 2019). Especially marine microorganisms such as bacteria and algae as well as their exudates are thought to be the source for the INPs. Connections to biological processes like plankton blooms have been made (Creamean et al., 2019). Another recent publication by Kirpes et al. (2019) found that locally produced open leads are the dominant aerosol source in winter. The emitted sea spray aerosol particles were found to possess organic coatings, consisting of marine saccharides, amino acids, fatty acids, and divalent cations. These substances are known from exopolymeric secretions produced by sea ice algae and bacteria, which, as mentioned before, are thought to be responsible for the ice activity in seawater. Studies on INPs at coastal sites tend to find influences from marine and terrestrial sources, often with a contribution of biological INPs and seasonal changes (Creamean et al., 2018; Šantl-Temkiv et al., 2019; Wex et al., 2019). For terrestrial sources, mineral dust itself is known to be relevant for lower temperatures (Sanchez-Marroquin et al., 2020), but Tobo et al. (2019) showed for glacial outwash material that dust can be the carrier for biological material, which is more ice active than the dust alone. Highly ice-active biological INPs have also been found in Arctic ice cores from up to 500 years ago (Hartmann et al., 2019). Also millennia-old permafrost soil was found to contain biological INPs that can be mobilized into the atmosphere, lakes, rivers, and the ocean when the Permafrost thaws (Creamean et al., 2020). This highlights the importance of biological INPs, especially in the changing Arctic environment.

Despite past significant efforts and increase in knowledge, we still lack quantitative insights concerning the abundance, the properties, and sources of Arctic INPs. Especially con-

cerning the last point, the relative importance of marine vs. terrestrial sources is still debated. Therefore, open questions addressed in this paper are outlined:

- What is the abundance of Arctic INPs and in what temperature range can they nucleate ice?
- What is the nature of Arctic INPs (biogenic material vs. mineral dust)?
- What is the origin of Arctic INPs (local vs. long range transport, marine vs. terrestrial)?

Our findings are constrained to the season and region in which measurements took place. They will nevertheless contribute to a better understanding concerning Arctic INPs and their potential effects on Arctic clouds. Furthermore, we provide valuable data for evaluating and driving atmospheric models in a region which is still heavily undersampled.

2 Methods

2.1 Campaign overview

The expedition PS106 of the research vessel *Polarstern* (Knust, 2017) was conducted between the end of May and mid-July 2017 in the Arctic Ocean (Wendisch et al., 2019). The measurements were performed as part of the PASCAL (Physical Feedbacks of Arctic Boundary Layer, Sea Ice, Cloud and Aerosol) campaign in the framework of the German Arctic Amplification: Climate Relevant Atmospheric and Surface Processes, and Feedback Mechanisms (AC)³ project.

The first leg (PS106.1) started on 24 May in Bremerhaven (Germany) and ended on 21 June in Longyearbyen (Svalbard) and featured a 10 d ice floe camp that was set up between 5 and 14 June 2017. The main area of investigation was the Arctic Ocean a few hundred kilometers northwest of Svalbard (see Fig. 1).

The expedition continued with its second leg (PS106.2) on 23 June from Longyearbyen and ended on 20 July in Tromsø (Norway). In comparison to PS106.1, the second leg focused on the area northeast of Svalbard, went up to higher latitudes (up to 83.7° N), and the vessel did not stop for extended stays at an ice floe.

As an overview about the meteorological situation during the campaign, Fig. S1 in the Supplement shows the frequency distributions for all meteorological parameters that were continuously measured on *Polarstern*. The mean and standard deviation of air temperature (T_{air}), relative humidity (RH), and atmospheric pressure (p) are given in the following: for the whole first leg they are $T_{\text{air}} = -0.01 \text{ °C} \pm 4.21 \text{ °C}$, $\text{RH} = 90.70 \% \pm 10.62 \%$, and $p = 1016.36 \text{ hPa} \pm 7.48 \text{ hPa}$, whereas for the second leg the parameters were $T_{\text{air}} = 0.22 \text{ °C} \pm 2.71 \text{ °C}$, $\text{RH} =$

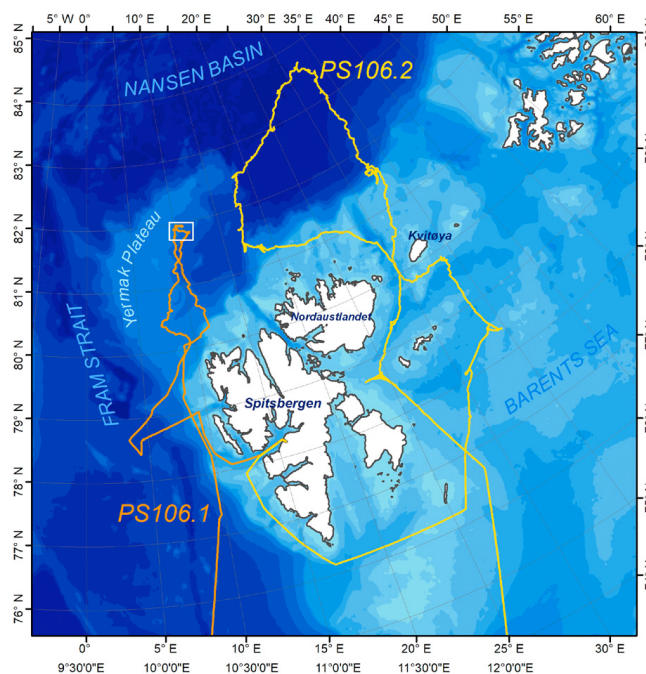


Figure 1. Overview of the main expedition area of the *Polarstern* cruises PS106.1 and PS106.2. Figure taken from Macke and Flores (2018).

$94.82 \% \pm 6.09 \%$, and $p = 1006.84 \text{ hPa} \pm 5.12 \text{ hPa}$. During the time within the ice pack, the averages of these parameters were as follows: $T_{\text{air}} = -1.37 \text{ °C} \pm 1.50 \text{ °C}$, $\text{RH} = 94.35 \% \pm 4.54 \%$, and $p = 1011.27 \text{ hPa} \pm 8.52 \text{ hPa}$; out of the ice pack, $T_{\text{air}} = 4.75 \text{ °C} \pm 3.65 \text{ °C}$, $\text{RH} = 88.03 \% \pm 11.27 \%$, and $p = 1012.92 \text{ hPa} \pm 4.89 \text{ hPa}$.

For further details on the measurement strategy as well as the meteorological, sea ice, and cloud conditions during PASCAL, we refer the reader to Wendisch et al. (2019) and the PS106 cruise report by Macke and Flores (2018).

2.2 Sample collection

In order to gain a comprehensive insight into the abundance and nature of INPs in the Arctic during summertime, samples from different compartments were taken. These included atmospheric, bulk seawater (BSW), sea surface microlayer (SML), and fog samples. All samples were stored on the vessel directly after sampling in a cold room at -20 °C , and it was ensured that the samples stayed below 0 °C during transport to the Leibniz Institute for Tropospheric Research (TROPOS), where they were stored at -24 °C until they were analyzed.

2.2.1 Filter sampling

Aerosol particles were sampled using a low-volume filter sampler (LVS; DPA14 SEQ LVS, DIGITEL Elektronik AG, Volketswil, Switzerland) with a PM_{10} inlet (DPM10/2.3/01,

DIGITEL Elektronik AG, Volketswil, Switzerland). The sampler was located on top of a measurement container placed on the starboard side of the monkey island (ca. 30 m above sea level). It was operated with an average volumetric flow of 27.9 L min^{-1} . It should be noted that our flow rate is lower than the standardized flow rate for PM_{10} inlets; hence, our cutoff diameter is higher than $10 \mu\text{m}$ (ca. $11.7 \mu\text{m}$). The LVS was routinely operated with an 8 h sampling period, which results in a total sampled air volume of 13.4 m^3 per filter sample. On 4 measurement days, the 8 h cycle was replaced by a 2 h cycle to study possible diurnal variation. The filter sampler features sealed storage cassettes and an automated filter change that allows for unsupervised sampling for multiple days. The samples were collected on polycarbonate pore filters (Nuclepore[®], Whatman[™]; $0.2 \mu\text{m}$ pore size, 47 mm diameter). Usually 12 filters were prepared and put in place inside the sampler. Two field blanks were taken on each leg and were used to define the lower limit of observable N_{INP} . A list of the almost 200 filter samples can be found in Table S1 in the Supplement. The filter-derived N_{INP} levels are also part of the overview of global shipborne INP measurements by Welti et al. (2020).

2.2.2 Bulk seawater and sea surface microlayer sampling

Seawater samples were taken from different environments, i.e., ice-free ocean, marginal ice zone (MIZ), open leads within the ice pack, or from melt ponds. In the case of the first three points, the samples were taken a few hundred meters away from the position of *Polarstern* using a Zodiac boat, while the melt ponds on the ice floe could be reached on foot. BSW samples were typically taken from a depth of 1 m with the help of a sealable bottle on a telescopic rod, with the exception of shallow melt ponds, where the samples were taken near the ground (for details, see Zeppenfeld et al., 2019). SML samples were collected with a glass plate sampler (Zeppenfeld et al., 2019; Van Pinxteren et al., 2017). The glass plate is dipped into the water body, slowly withdrawn, and the surface film, which clings to the sides of the glass plate, is wiped off the plate into a sample container with a Teflon[®] wiper.

The seawater sampling was conducted on a daily basis. The SML and bulk seawater samples were taken at the same time and location with the only exceptions being shallow melt ponds where no samples from 1 m depth could be taken as well as days with harsh weather when no surface film could form; 42 SML samples and 42 bulk seawater samples were collected during the campaign. A further description of the seawater sampling and a chemical and microbiological analysis of the samples can be found in Zeppenfeld et al. (2019). A list of the seawater samples can be found in Table S2 in the Supplement.

2.2.3 Fog sampling

Fog was collected with the Caltech Active Strand Cloud Collector Version 2 (CASCC2; described in Demoz et al., 1996). The CASCC2 is a non-selective sampler that catches hydrometeors by impaction on Teflon[®] strands ($508 \mu\text{m}$ diameter). Droplets caught on the strands are gravitationally channeled into a Nalgene bottle. The instrument operates with a flow rate of approximately $5.3 \text{ m}^3 \text{ min}^{-1}$, resulting in a 50 % lower cutoff size of approximately $3.5 \mu\text{m}$. During daytime on leg 1 the sampler turned on every time the visibility decreased significantly and was running continuously during the night. On leg 2 the sampler was running continuously, and the sample bottle was changed whenever a significant amount of sample material was collected and after the fog event was over. In all cases the sampler was rinsed with ultrapure water after a fog event was sampled and after the sample bottle was changed. During the entire campaign, 22 samples were collected, with about two-thirds of them on the second leg alone. A list of all fog samples can be found in Table S3 in the Supplement.

2.3 INP analysis

2.3.1 Sample preparation

Samples stored at -24°C were thawed only to perform the measurements. The measurements were performed on the same day as the thawing, and the remaining sample material was refrozen at the end of the day on which the measurements were completed.

The polycarbonate filters were put in a centrifuge tube along with 3 mL of ultrapure water (type 1; Direct-Q[®] 3 water purification system, Merck Millipore, Darmstadt, Germany) and were shaken in an oscillating shaker for 15 min in order to extract the particles from the filter and bring them into suspension. Then 100 μL of that suspension was removed for the analysis with the Leipzig ice nucleation array (LINA; described in Sect. 2.3.3). For the analysis with the ice nucleation droplet array (INDA; described in the Sect. 2.3.4), the remaining 2.9 μL of the suspension was made up to a total of 6 mL with ultrapure water and shaken again as before. The reason for this procedure is to use as little water as viable, i.e., to dilute the sample as little as possible.

Sea and fog water samples did not require any preparation and could be directly measured with either setup.

2.3.2 Test for heat-labile INPs

After the initial measurement, arbitrarily selected samples were chosen to test for the presence of heat-labile INPs in the samples. The sample solution was sealed in a centrifuge tube and placed in an oven. The sample was heated at 95°C for 1 h and subsequently analyzed with the LINA device (described in Sect. 2.3.3).

2.3.3 Leipzig ice nucleation array (LINA)

LINA is a droplet-freezing assay (DFA), the design of which is based on a DFA called BINARY by Budke and Koop (2015). An array of 90 droplets with a typical volume of 1 μL of the sample suspension is placed onto a hydrophobic glass slide (40 mm diameter). Each droplet is within its individual compartment made from a perforated, anodized aluminum plate and covered with another glass slide. In this way it can be ensured that droplets do not interact during the freezing process, e.g., via ice seeding by frost splintering or the Bergeron–Wegener–Findeisen process. Furthermore, droplet evaporation is minimized. At a cooling rate of 1 $^{\circ}\text{C min}^{-1}$, the sample droplets are cooled by a 40 \times 40 mm² Peltier element inside a freezing stage (LTS120, Linkam Scientific Instruments, Waterfield, UK). The freezing stage is coupled with a cryogenic water circulator (F25-HL, Julabo, Seelbach, Germany) in order to achieve temperatures below -25°C down to the temperature at which homogeneous freezing occurs naturally, i.e., -38°C . A thin layer of squalene oil thermally connects the Peltier element and the glass slide with the droplets on top. The freezing stage itself consists of a gas-tight aluminum housing, which is purged with dry particle-free air during the measurement. LED dome lighting (SDL-10-WT, MBI-Imaging GmbH, Hamburg, Germany) is used for shadow-free illumination of the droplets. A charge-coupled device camera is mounted at the apex of the dome and takes images every 6 s, which corresponds to a temperature resolution of 0.1 $^{\circ}\text{C}$ if cooled with 1 $^{\circ}\text{C min}^{-1}$. An aperture below the dome blocks the light partially and creates a ring-shaped reflection in each droplet. This is used as a detectable feature that vanishes upon freezing of the droplet. A custom Python algorithm then evaluates each image in terms of the number of frozen droplets, N_f , in each individual image. As every image corresponds to a certain temperature, the frozen fraction at the respective temperature, $f_{\text{ice}}(T)$, can be easily derived. LINA was used to evaluate all filter samples as well as all SML and BSW samples.

2.3.4 Ice nucleation droplet array (INDA)

The basic design of the INDA device is inspired by Conen et al. (2012), but as suggested in Hill et al. (2016), polymerase chain reaction (PCR) plates instead of individual tubes were used. In each of the 96 wells of the PCR plate, 50 μL of sample material was filled. Then the PCR plate was sealed with a transparent cover foil and immersed in the bath of a cryostat (FP45-HL, Julabo, Seelbach, Germany) in a way that the wells themselves were surrounded by refrigerant (ethanol) but not so deep that the PCR plate would be completely submerged. The PCR plate was illuminated from below, which makes the phase change of the sample suspension visible as a darkening of the respective well. The temperature of the refrigerant was lowered with a rate of ca. 1 $^{\circ}\text{C min}^{-1}$ while simultaneously the temperature was recorded, and a

top-mounted camera took pictures at 0.1 $^{\circ}\text{C}$ intervals. The images were then again evaluated with a custom Python algorithm for N_f in order to derive $f_{\text{ice}}(T)$. INDA was used for measurements of SML and BSW samples as well as for fog water.

2.3.5 INP number concentrations N_{INP}

Cumulative number concentrations of INPs per volume of sample as a function of temperature were calculated for each experiment utilizing the equation given in Vali (1971):

$$N_{\text{INP}}(T) = \frac{-\ln(1 - f_{\text{ice}})}{V_{\text{drop}}} \quad (1)$$

with $f_{\text{ice}} = \frac{N_{\text{frozen}}(T)}{N_{\text{total}}}$, where N_{total} is the number of droplets, and $N_{\text{frozen}}(T)$ is the number of frozen droplets at temperature T . With the given number of droplets ($N_{\text{total}} = 90$) and volume ($V_{\text{drop}} = 1 \mu\text{L}$), the upper and lower limits of the detectable range of LINA are 1.12×10^4 and $4.5 \times 10^6 \text{ L}^{-1}$ (water), respectively, whereas 2.1×10^2 and $9.1 \times 10^4 \text{ L}^{-1}$ (water), respectively, are the limits for INDA ($N_{\text{total}} = 96$; $V_{\text{drop}} = 50 \mu\text{L}$). The temperature values of the seawater samples were corrected for freezing-point depression due to the salt content as described in Koop and Zobrist (2009).

In the case of the atmospheric filter samples in order to derive atmospheric N_{INP} , the denominator in Eq. (1) needs to be modified so that it represents the volume of air distributed in each droplet:

$$N_{\text{INP}}(T) = \frac{-\ln(1 - f_{\text{ice}})}{\frac{V_{\text{air}}}{V_{\text{wash}}} \cdot V_{\text{drop}}}, \quad (2)$$

where V_{air} is the air volume sampled onto one filter, and V_{wash} is the volume of water that the particles were rinsed off with and suspended in.

The uncertainty in N_{INP} was calculated with a formula by Agresti and Coull (1998). Agresti and Coull (1998) published an approximation for binomial sampling intervals, which was applied to N_{INP} measurements by, for example, Gong et al. (2020), McCluskey et al. (2018a), and Hill et al. (2016). Following their approach, the confidence intervals for f_{ice} are calculated by

$$\left(f_{\text{ice}} + \frac{z_{a/2}^2}{2n} \pm z_{a/2} \sqrt{\left[f_{\text{ice}}(1 - f_{\text{ice}}) + \frac{z_{a/2}^2}{4n} \right] / n} \right) / \left(1 + \frac{z_{a/2}^2}{n} \right), \quad (3)$$

where n is the droplet number, and $z_{a/2}$ is the standard score at a confidence level $a/2$, which for a 95 % confidence interval is 1.96.

2.4 Collocated measurements and supporting observations

In addition to the sampling of INPs, the physicochemical properties of the prevailing atmospheric aerosol particles

were measured inside a temperature-controlled measurement container located on the monkey island of the RV *Polarstern*. The temperature inside the container was held at ca. 24 °C, while the aerosol inlet was heated to 30 °C to prevent icing. The aerosol inlet consists of a 6 m long stainless-steel tubing (inner diameter of 40 mm), which faces upwards at a 45° angle to the bow of the ship. The flow through the inlet was set to 40 L min⁻¹ (Reynolds number < 2000). With an isokinetic splitter, the aerosol was distributed between the different instruments. The aerosol instrumentation relevant to this study included a mobility particle size spectrometer (MPSS) to measure particle number size distributions (PNSDs), a condensation particle counter (CPC) to measure total particle concentration (N_{tot}), and a cloud condensation nuclei counter (CCNC) to measure the concentrations of cloud condensation nuclei (N_{CCN}).

PNSDs in the size range between 10 and 800 nm were measured with a TROPOS-type MPSS (Wiedensohler et al., 2012). The time resolution of an upscan and downscan was 5 min. PNSDs were derived with the inversion algorithm by Pfeifer et al. (2014) and corrected for transmission losses as well as counting efficiencies according to Wiedensohler et al. (1997). The sizing of the MPSS was calibrated according to Wiedensohler et al. (2018) at regular time intervals during the campaign (for further details on the MPSS and the measurement container, we refer the reader to Kecorius et al., 2019). N_{tot} was measured with a CPC (model 3010, TSI Inc., Shoreview, USA; lower cutoff: 10 nm). A CCNC (CCN-100, DMT, Boulder USA; Roberts and Nenes, 2005) was used to measure N_{CCN} at six different supersaturation values (SS: 0.1 %, 0.15 %, 0.2 %, 0.3 %, 0.5 %, 1 %). Each SS level was sampled for 10 min and averaged over that period; hence, a certain SS has a time resolution of 1 h. The instrument was calibrated with ammonium sulfate particles before and after the campaign according to the ACTRIS protocol (Gysel and Stratmann, 2013).

In addition to the offline INP analysis of the filter samples, also the SPectrometer for Ice Nuclei (SPIN; Droplet Measurements Techniques, Boulder, CO, USA) was deployed to measure N_{INP} in immersion mode online. SPIN is a continuous-flow diffusion chamber (CFDC) with a parallel plate geometry, and the measurement principle of SPIN in immersion mode can be briefly described as follows: aerosol particles are activated to cloud droplets and then exposed to conditions where ice can form. The number of formed ice crystals is then optically detected. SPIN is described in detail in Garimella et al. (2016). SPIN was placed within a measurement container. Together with the other aerosol instrumentation, the aerosol was fed to SPIN through one main inlet but with additional subsequent drying of the aerosol. SPIN sampled in half-hourly intervals of constant temperature and relative humidity, and each sampling condition was repeated three times within 24 h. The SPIN dataset is also part of the overview of global shipborne INP measurements by Welti et al. (2020).

Na⁺ and Cl⁻ mass concentrations on size-resolved ambient aerosol particles were measured from five-stage Berner impactor samples (mounted outside of the measurement container; the setup is described in detail in Kecorius et al., 2019) by ion chromatography (ICS3000, Dionex, Sunnyvale, CA, USA), as described in Müller et al. (2010) in more detail. Ion chromatography was also used to determine the salinity of the seawater samples.

5 d air mass back-trajectories were calculated using the HYbrid Single-Particle Lagrangian Integrated Trajectory (HYSPLIT) model (Rolph et al., 2017; Stein et al., 2015). As input for the model, the GDAS1 meteorological fields (Global Data Assimilation System; 1° latitude/longitude; 3-hourly) were used. Trajectories were initiated at 50, 250, and 1000 m every hour.

The sea ice concentration at the position of *Polarstern* was determined with the sea ice concentration product of the EU-METSAT Ocean and Sea Ice Satellite Application Facility (OSI-401-b: SSMIS Sea Ice Concentration Maps on 10 km Polar Stereographic Grid; Tonboe et al., 2017).

Chlorophyll *a* (Chl *a*) concentration was derived from the vessel's FerryBox system (4H-FerryBox, Jena Engineering, Jena, Germany). A FerryBox is an autonomous online instrument with modular sensor assembly to continuously measure oceanographic parameters in a flow-through system (Petersen et al., 2011, 2007). The data from the Chl *a* sensor in the FerryBox system were accessed via the DSHIP portal (<https://dship.awi.de/>, last access: 26 March 2021) provided by the operator of the vessel. Chl *a* concentrations were also derived from satellite remote sensing (Aqua MODIS, NPP, L3SMI, Global, 4 km, Science Quality, 2003–present, 8 d composite, 8 to 16 July).

3 Results and discussion

3.1 Atmospheric INP concentrations N_{INP}

A time series of atmospheric N_{INP} at selected temperatures derived from filter samples and online measurements with SPIN is shown in Fig. 2. The colored areas mark the periods when *Polarstern* was located in a certain environment (yellow = ice-free ocean; blue = within ice pack; purple = marginal ice zone). Overall N_{INP} is the highest at the beginning of the campaign, in between both legs at the harbor of Longyearbyen, and upon entering the ice-free ocean again towards the end of the second leg. The lowest concentrations occurred when the vessel was within the ice pack. It can also be seen that, at a given time, peaks appear or disappear depending on temperature, indicating that different populations of INPs contribute at warmer or colder temperatures.

Figure 3 shows the N_{INP} freezing spectra for the atmospheric filter samples measured with LINA (circle markers), as well as $N_{\text{INP}}(T)$ measured with SPIN (cross markers). The color represents the environment in which the sampling

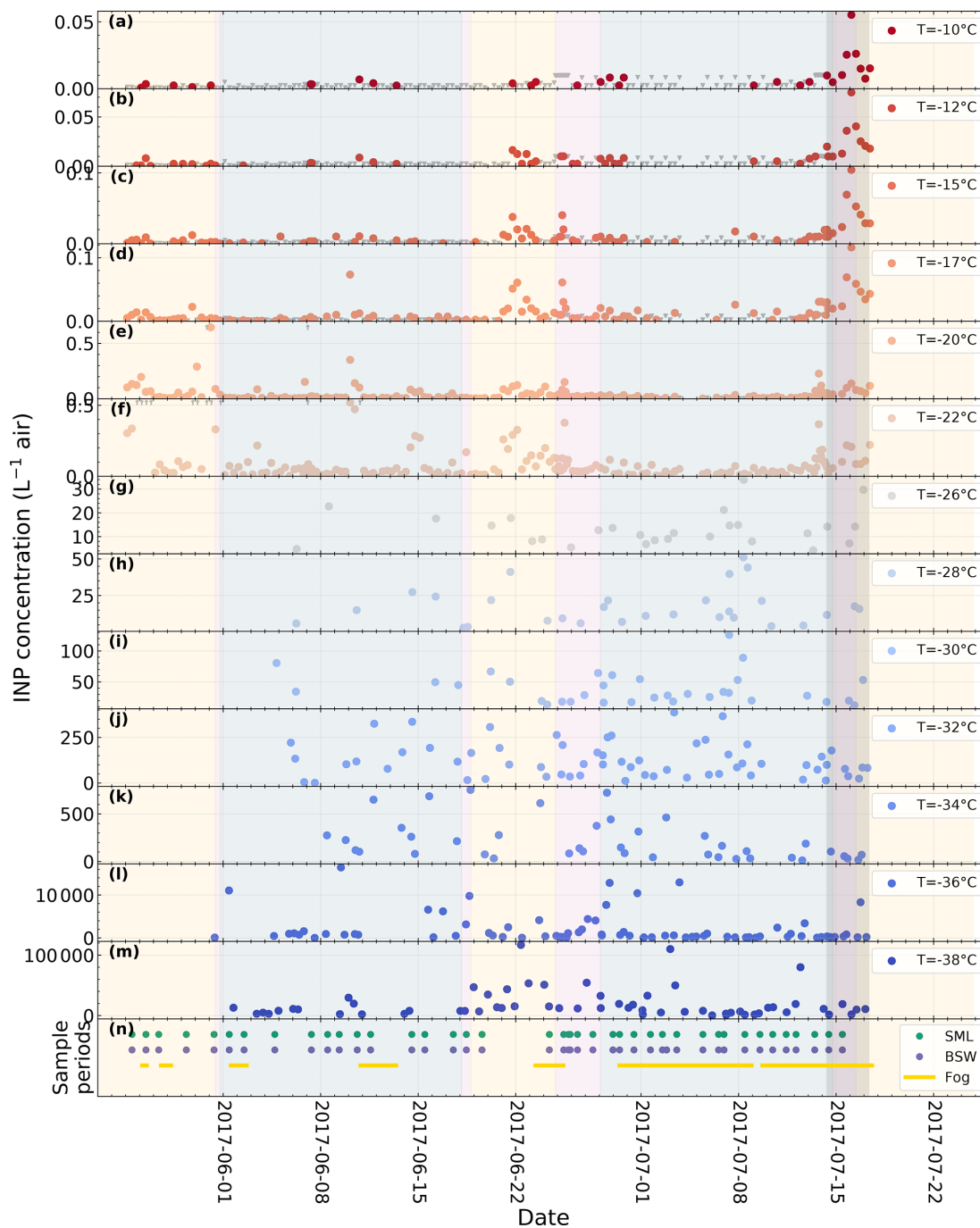


Figure 2. Time series of atmospheric N_{INP} at different temperature derived from filter samples with LINA ($-22^{\circ}C$ and above) and SPIN measurements ($-26^{\circ}C$ and below). The bottom panel contains markers for the sample collection times of the SML, BSW, and fog water samples. The shaded areas indicate the environment that the vessel is located in (yellow = ice-free ocean; blue = within ice pack; purple = marginal ice zone). The dark gray area indicates the period of the case study discussed in Sect. 3.5. Note that SPIN measurements were only obtained beginning with 31 May.

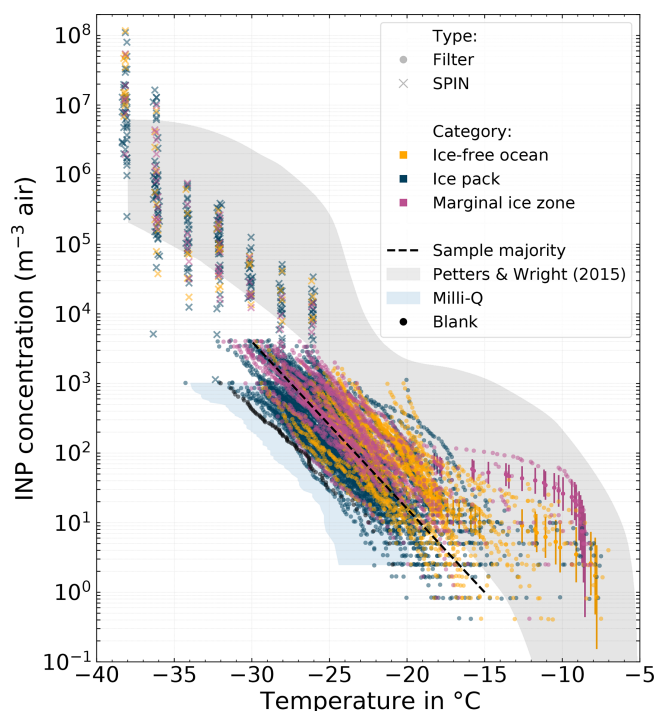


Figure 3. All cumulative INP spectra derived from atmospheric filter samples measured with LINA (circle marker), as well as $N_{\text{INP}}(T)$ measured with SPIN (cross marker). The color code refers to the environment the sample was taken from (yellow = ice-free ocean; blue = ice pack; purple = marginal ice zone). The majority of the filter samples are clustered around a line which is shown as a black dashed line. The range of N_{INP} for midlatitudes by Petters and Wright (2015) is shown as a gray shaded area for reference. The blue areas depicts the 10th to 90th percentile range of all pure Milli-Q measurements with LINA (scaled to atmospheric concentrations with the average sampled air volume of the 8 h samples).

took place, based on the sea ice concentrations at the location of *Polarstern* (yellow = ice-free ocean; blue = ice pack; purple = marginal ice zone, MIZ). The MIZ is defined as the transitional zone between open sea and dense drift ice. It spans from 15 % to 80 % of the sea surface being covered with ice. The area north of the MIZ is classified as the ice pack, and the area south of the MIZ is classified as ice-free ocean. As the filter samples were collected over the course of several hours on an often moving vessel, the sample environment might change during sampling. In such cases the sample was labeled according to the environment, which accounts for most of the sampling time. The range of N_{INP} for midlatitudes by Petters and Wright (2015) is shown as a gray shaded area for reference. Additionally, Fig. S10 in the Supplement shows a box plot of the very same filter samples, in order to emphasize the general differences between the environments.

At any particular temperature, N_{INP} varies between 2 to 3 orders of magnitude. The variability tends to be higher at warmer temperatures compared to colder temperatures: at

-10°C N_{INP} varies between 4×10^{-1} and $6 \times 10^1 \text{ m}^{-3}$, at -17°C between 4×10^{-1} and $1 \times 10^2 \text{ m}^{-3}$, and at -25°C between 3×10^1 and $2 \times 10^3 \text{ m}^{-3}$. It can be seen that the majority of the samples are clustered around a line ranging roughly from 1 m^{-3} at -15°C to $4 \times 10^3 \text{ m}^{-3}$ at -30°C . But also highly ice-active filter samples featuring N_{INP} as high as $6 \times 10^1 \text{ m}^{-3}$ at -10°C were observed. These tend to be associated more often with the MIZ (purple symbols) and at -15°C also with the ice-free ocean (yellow symbols) environment than with the ice pack (see Fig. S10 in the Supplement). We will describe these highly ice-active samples in more detail in Sect. 3.5. In comparison to the range of N_{INP} from midlatitudes by Petters and Wright (2015), the filter-derived N_{INP} levels are lower for temperatures below ca. -20°C , but similar at warmer temperatures. For a given temperature, N_{INP} measured with SPIN falls within the lower half of the N_{INP} range by Petters and Wright (2015), with the exception of the two lowest temperature steps.

In Fig. 3 it can be seen that some LINA freezing spectra go up to higher values ($4 \times 10^3 \text{ m}^{-3}$) than others (ending at $1 \times 10^3 \text{ m}^{-3}$). The cause of this lies in the measurement principle itself: DFAs only measure N_{INP} per volume of water in a certain concentration range determined by the specific setup configuration. With the known volume of air sampled onto one filter, these concentrations per volume of water are then scaled to atmospheric concentrations per volume of air. Hence differing ranges of resulting values are caused by systematic differences in V_{air} . In our case we collected samples for 8 or 2 h, and since the flow rate is relatively constant, V_{air} of the 8 h samples is about 4 times larger than that of the 2 h samples, which causes also the different reported ranges in atmospheric N_{INP} as seen in Fig. 3. It should also be mentioned that the upper and lower ends of the freezing spectra shown in this work only represent the limits of our detectable range and do not imply that outside these limits no higher N_{INP} or lower N_{INP} existed.

The test for heat-labile INPs (Figs. S6 and S7 in the Supplement) demonstrates that ice activity of the samples is reduced when heated for 1 h at 95°C . Especially INPs that nucleated ice at temperatures above ca. -16°C are gone after the heating. This is widely seen as an indicator for the presence of biogenic, proteinaceous INPs as those become denatured during the heating, which reduces their ice activity (Conen et al., 2011, 2012, 2017; Conen and Yakutin, 2018; Felgitsch et al., 2018; Hara et al., 2016; Joly et al., 2014; Moffett et al., 2018; Hill et al., 2016; Huang et al., 2021; McCluskey et al., 2018b; Kunert et al., 2019; Pouleur et al., 1992).

In the previous section we described that at warmer temperatures, e.g., at -10°C , samples with high INP concentrations are found more often in the MIZ and less frequently within the ice pack. In comparison, at the lower temperatures measured with SPIN (cross markers in Fig. 4) no correlation with the environmental setting is found. However, in a global context the level of N_{INP} at these low temperatures is

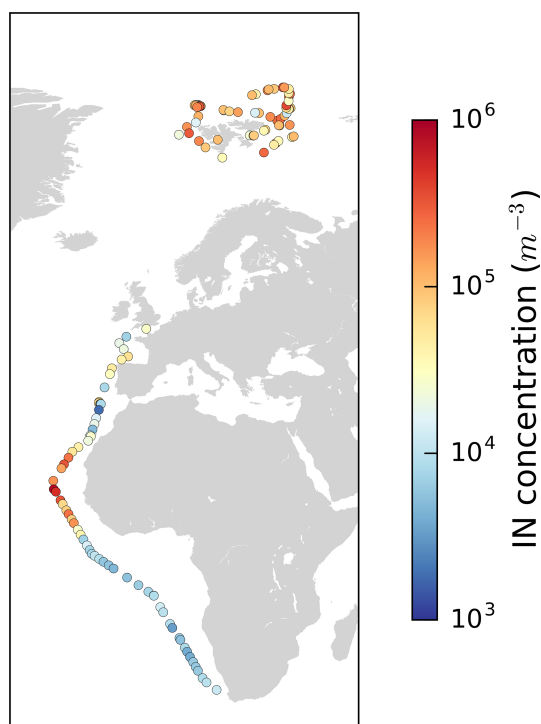


Figure 4. Map with color-coded N_{INP} in the Arctic at -32°C measured with SPIN during PS106 and also SPIN data of a transect from Bremerhaven (Germany) to Cape Town (South Africa) along the western coast of Africa (Welti et al., 2020).

remarkable by itself as shown in Fig. 4. That figure shows N_{INP} in the Arctic at -32°C measured with SPIN during PS106 but also SPIN data by Welti et al. (2020) of a transect from Bremerhaven (Germany) to Cape Town (South Africa) along the western coast of Africa. It is striking that at these low temperatures N_{INP} levels in the Arctic are in the same order of magnitude as in the outflow region of mineral dust from the Sahara. While we have no means of proving the presence of mineral dust at these colder temperatures during PASCAL, to our knowledge there are also no other known sources of INP that can produce such high concentrations throughout the whole time period of the campaign. Also, it was recently shown by Sanchez-Marroquin et al. (2020) that Iceland can be a strong Arctic dust source. Also Irish et al. (2019a) suggested that observed INPs were mineral dust particles originating in the Arctic (Hudson Bay, eastern Greenland, northwest continental Canada) rather than particles originating from sea spray. And global model transport simulations done by Groot Zwaafink et al. (2016) show that mineral dust is not only transported into the Arctic from remote regions but also, possibly increasingly, generated in the region itself. However, it is also possible also other sources of mineral INPs contribute to the INP population at these temperatures. For example, diatoms represent a biogenic but mineral source of INPs, as they have a cell wall made of silica (Xi et al., 2021). Therefore, it is likely that mineral INPs,

possibly mineral dust, contribute to N_{INP} at low temperatures during the campaign.

3.2 INPs in sea surface microlayer and bulk seawater

Figure 5 shows N_{INP} per volume of water in SML and BSW. Again, the color code refers to the environment the sample was taken from (yellow = ice-free ocean; blue = ice pack; purple = MIZ; green = melt point). The gray box indicates the range of values reported in an earlier study by Wilson et al. (2015) in the Arctic, although they did not separate their samples into different environments. Additionally, Figs. S11 and S12 in the Supplement show box plots of the very same SML and BSW samples in order to emphasize the general differences between the environments.

Both SML and BSW show a high intersample variability. Concentrations for both vary at least between 2 and 3 orders of magnitude at any temperature. Some samples initiate freezing clearly above -10°C (highest observed freezing onset was at -5.5°C), while for other samples freezing starts only at temperatures below -15°C .

It is worth mentioning that the concentration range of INPs reported by Wilson et al. (2015) is not directly comparable to the measurements we present, because due to a different measurement setup, they have different limits of their detectable range. Nevertheless, it can be seen that their SML samples contain up to 2 orders of magnitude higher concentrations of INPs that are ice active at high temperatures (above ca. -10°C).

Interestingly, some of our samples stand out, i.e., feature significantly higher ice activities at a certain temperature than the majority of the samples (see Fig. 5). The dashed black line in Fig. 5 roughly separates the samples into those that stand out (above the line) and the rest of the very similar samples (below the line). It is noticeable that SML samples from the known biologically active MIZ belong mostly to the group of samples that stand out from the rest. Also the overall most active SML sample originates from the MIZ, and its connection to the corresponding atmospheric filter samples is discussed in more detail in the case study in Sect. 3.5. The high variability of the INP concentrations in SML and BSW in our view is a clear hint towards the sporadic occurrence of INPs in these compartments.

The SML has been found to be enriched in particulate organic matter and surface-active substances compared to the underlying bulk seawater, with enrichment factors (EFs) of up to 10 and 50, respectively, being reported (Engel et al., 2017; Kuznetsova and Lee, 2002). And, as described in the introduction, the SML is known to be highly ice active. It is therefore an interesting question whether INPs are also enriched in the SML compared to BSW and whether enrichment is a general feature in all samples or if it is restricted to certain situations. To answer this question, we derived INP enrichment factors for the SML, based on correspond-

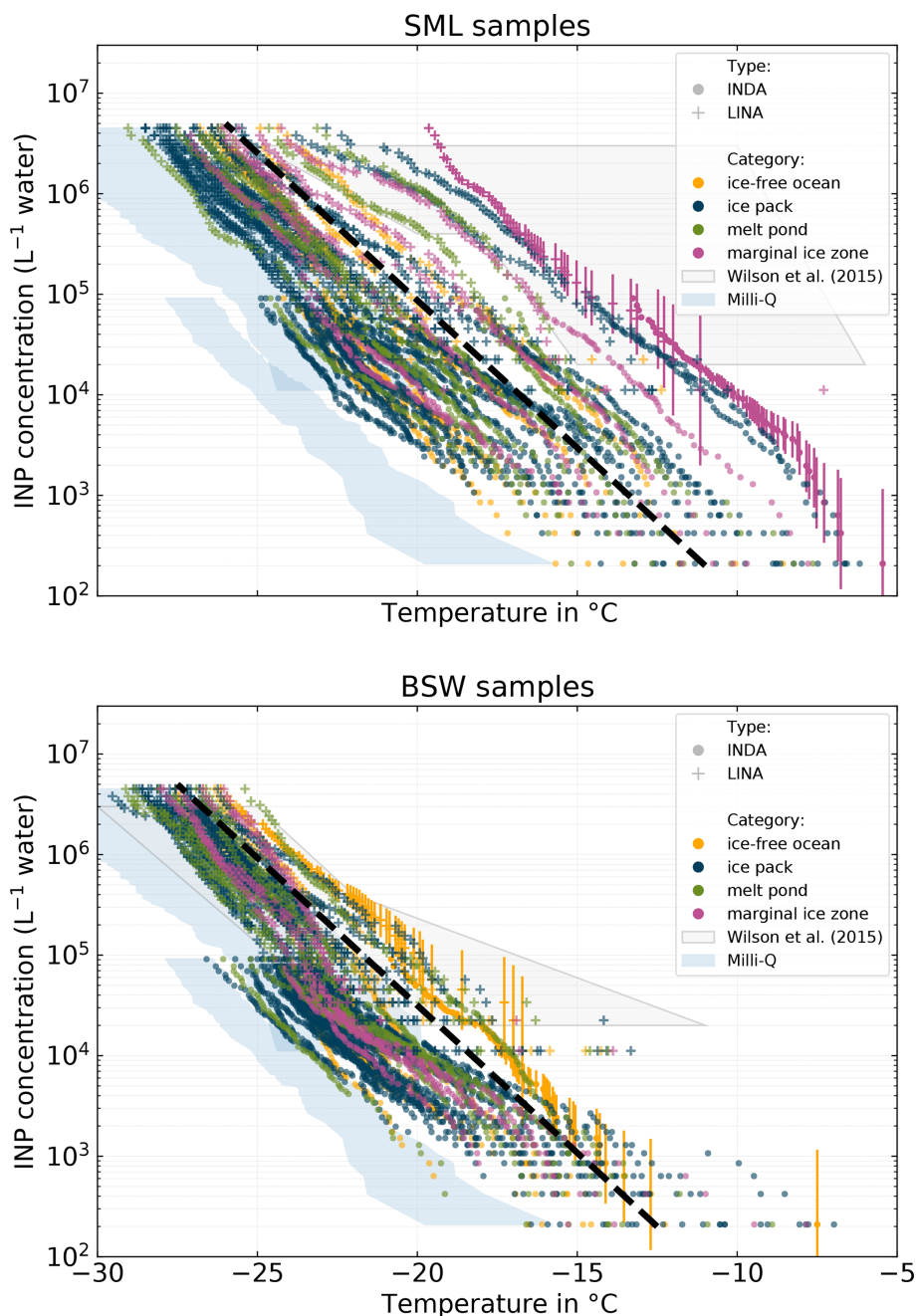


Figure 5. N_{INP} in SML and BSW measured with INDA and LINA. Samples are categorized according to the environment (ice-free ocean, ice pack, melt pond, marginal ice zone) the samples were taken from. The gray box indicates the range of values reported by Wilson et al. (2015) for the Arctic. The blue areas depicts the 10th to 90th percentile range of all pure Milli-Q measurements with INDA and LINA.

ing SML and BSW samples as

$$\text{EF}_{\text{INP}}(T) = \frac{N_{\text{INP, SML}}(T)}{N_{\text{INP, BSW}}(T)}. \quad (4)$$

Figure 6 depicts the calculated EFs at selected temperatures. We observe that the majority of SML samples are enriched in INPs compared to the underlying BSW. The majority of EFs fall into the range between 1 and 10, with only four oc-

currences of higher values. The highest EF we found was 94.97. There are seven occurrences of $\text{EF} = 1$ and only one of $\text{EF} \leq 1$. This result is similar to Wilson et al. (2015), who only observed enrichment and no depletion of INPs in the SML. On the other hand, the study by Irish et al. (2017) also reports few cases of INPs depletion in the SML. But, as Gong et al. (2020) pointed out, direct comparisons of EFs

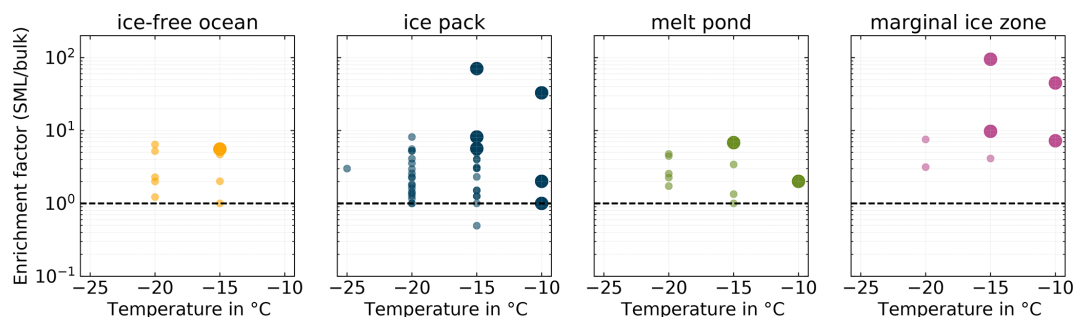


Figure 6. Enrichment factors for all pairs of SML and BSW samples (INDA measurements) divided into separate panels by their environmental setting. Larger markers correspond to the pairs of samples for which either the SML or the BSW sample stands out in terms of ice activity.

between different studies are difficult since methodological differences might be of importance.

The larger markers in Fig. 6 indicate samples where the SML showed significantly higher ice activity compared to the others, i.e., higher INP concentrations (see above). Interestingly, almost exclusively the highly ice-active SML samples are the samples which feature the highest EFs, suggesting that enrichment could be an important factor in controlling SML ice activity.

Filtrations of 10 randomly selected SML and 12 BSW samples were created and analyzed for N_{INP} to find indications concerning the size of the INPs present in the samples. The samples were filtered with $0.2\ \mu\text{m}$ PTFE syringe filters (Puradisc 25, Whatman). While the individual sample was chosen randomly, it was ensured that all sample environments (ice-free ocean, ice pack, melt pond, marginal ice zone) were considered. Figure 7 shows a scatter plot of the T_{10} values, i.e., the temperature where 10 % of the droplets are frozen, of the filtered and unfiltered samples. If a sample falls below the 1 : 1 line, it indicates that the filtration reduced the ice activity, and the distance to the 1 : 1 line in the x direction is a measure of how strong the reduction in ice activity is. The complementary plots of the T_{50} and T_{90} can be found in the Supplement. Throughout all samples a reduction of the freezing temperatures can be seen due to filtrations. Also, the more ice active the unfiltered sample was, the larger the shift towards lower temperatures tends to be (see also Fig. S4 in the Supplement). The most ice-active sample shifted by around $5\ ^\circ\text{C}$, while those with lower initial ice activity only are decreased by approximately $2\ ^\circ\text{C}$. This clearly indicates that a high fraction of the INPs are larger or at least associated with particles larger than $0.2\ \mu\text{m}$.

3.3 INPs in fog water

Analogous to the SML and BSW samples, N_{INP} was also determined in collected fog water samples. At $-10\ ^\circ\text{C}$, we find N_{INP} between the lower limit of our detectable range of 2×10^2 and $2 \times 10^4\ \text{L}^{-1}$. At $-15\ ^\circ\text{C}$, N_{INP} between $6 \times 10^2\ \text{L}^{-1}$ and the upper limit of our detectable range $9 \times 10^4\ \text{L}^{-1}$ were

observed. At $-20\ ^\circ\text{C}$, values between $1 \times 10^4\ \text{L}^{-1}$ and the upper limit of our detectable range, $9 \times 10^4\ \text{L}^{-1}$ were found. Fourteen fog samples (63.6 % of all fog samples) have a freezing onset above $-10\ ^\circ\text{C}$, suggesting the presence of biogenic INPs, as mineral dust only starts to contribute to the INP population at temperatures below $-15\ ^\circ\text{C}$ (e.g., Murray et al., 2012; O’Sullivan et al., 2018). The highest freezing onset we observed in a sample was at $-3.47\ ^\circ\text{C}$. The samples are divided into two groups by a clearly recognizable gap. The occurrence of these two groups could not directly be related to meteorological parameters. However, as will be discussed in Sect. 3.3.1, the group of more ice-active fog samples may be associated with the more ice-active atmospheric filter samples.

In general the fog samples tend to be more ice active and show higher N_{INP} at a given temperature than the seawater samples presented in Sect. 3.2. A qualitatively similar observation was already made by Schnell (1977). For seawater samples that they collected near Nova Scotia (Canada), they found that some of the samples were very ice active, although the majority of their seawater samples contained no INPs active at temperatures warmer than $-14\ ^\circ\text{C}$. On the other hand, half of their fog water samples were ice active at temperatures above $-10\ ^\circ\text{C}$ with the most ice-active sample initiating freezing at $-2\ ^\circ\text{C}$. Schnell (1977) also described that they found N_{INP} in seawater, fog, and air to vary independently from each other. An observation that also largely applies to this study, but a more detailed investigation of the relation between N_{INP} in the different compartments is presented in the following Sect. 3.3.1 and 3.4.

The $N_{\text{INP}}(T)$ we observed in Arctic fog water is similar to what Gong et al. (2020) found in cloud water samples on the Cabo Verde islands but tends to be lower than what was observed by Joly et al. (2014), who measured at Puy-de-Dôme (France) and reported a correlation between high concentrations of biological particles and INP concentrations. However the freezing onset temperature of around $-6\ ^\circ\text{C}$ is almost identical in the three studies.

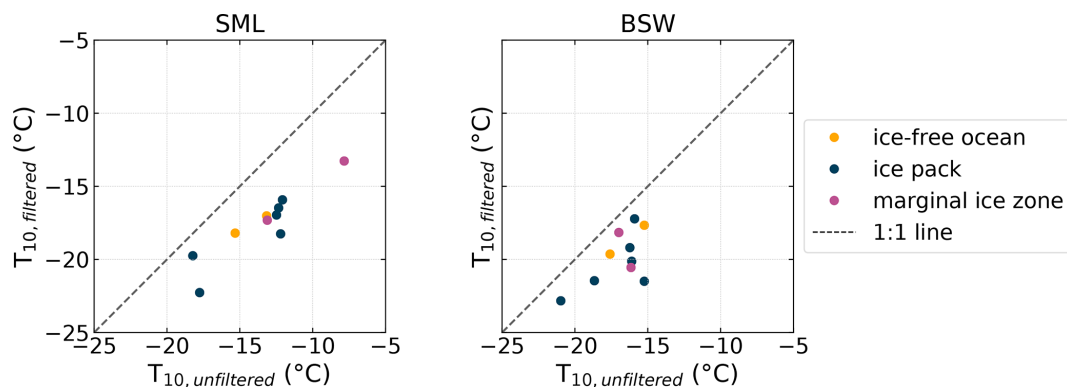


Figure 7. Comparison of filtered and unfiltered SML and BSW samples measured with INDA. Shown are the T_{10} values for corresponding samples. Symbols below the 1 : 1 line indicate that the filtered sample is less ice active.

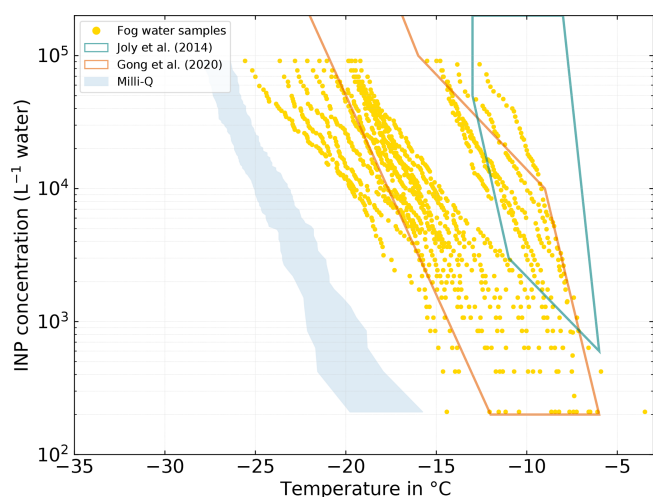


Figure 8. N_{INP} in fog water samples measured with INDA. The teal and orange polygons show the range of values observed by Joly et al. (2014) and Gong et al. (2020), respectively.

3.3.1 Connecting INPs in clear or fog-free air to fog samples

In this section we relate and compare N_{INP} in fog water samples with those measured in fog-free air (see Sect. 3.1), following the procedure introduced in Gong et al. (2020), which is briefly described in the following. The number concentration of CCN (N_{CCN}) at a particular supersaturation (SS) is used as a proxy for the fog droplet number concentration. Furthermore, Gong et al. (2020) made the legitimate assumption, that all INPs act as CCN. Together with an estimated fog droplet diameter (d_{drop}), the volume of fog water per volume dry air, LWC_{fog} , can be calculated as follows:

$$\text{LWC}_{\text{fog}} = N_{\text{CCN}} \cdot \pi/6 \cdot d_{\text{drop}}^3. \quad (5)$$

For determining N_{CCN} , a SS needs to be defined. Since fog, unlike clouds, is characterized by low updrafts, SS is also

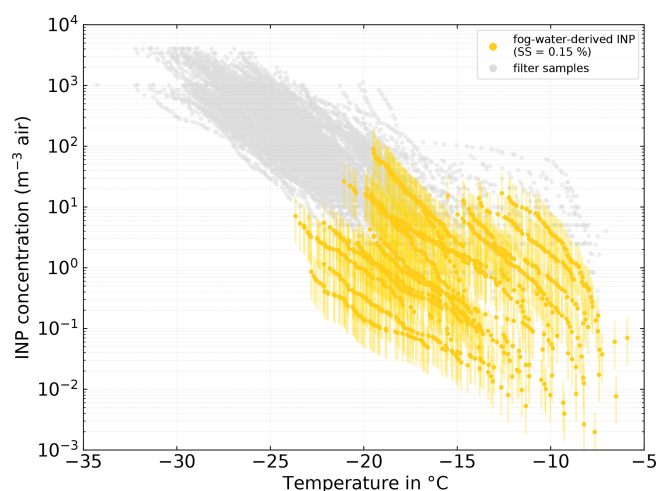


Figure 9. Fog-water-derived N_{INP} in air. N_{INP} was derived from Eqs. (5) and (6) with the median N_{CCN} (SS = 0.15 %) during the time of each fog sample and an average droplet diameter (d_{drop}) of 17 μm . The error bars show the range with d_{drop} of 12 and 22 μm , respectively. See Sect. 3.3.1 for details on the derivation method.

typically low (0.02 %–0.2 %; Pruppacher and Klett, 2010). Thus we choose N_{CCN} measured at SS = 0.15 % as a proxy for the droplet number concentration. Please note that we do not use N_{CCN} measured at SS = 0.1 %, because after the removal of data points due to quality assurance, the data coverage for SS = 0.15 % is significantly better than for SS = 0.1 %.

Remote sensing studies of Arctic cloud droplet sizes report typical diameters between 14 and 20 μm (Bierwirth et al., 2013; Shupe et al., 2001; King et al., 2004) and in situ observations found values between 12 and 22 μm . Hence we use 17 μm as an average d_{drop} and vary it between 12 and 22 μm . With that we calculate a range of LWC_{fog} , which is then further used to derive the INP number concentration in air, $N_{\text{INP,air}}$, based on the INP concentration in fog water,

$$N_{\text{INP, fogwater}}$$

$$N_{\text{INP, air}} = \text{LWC}_{\text{fog}} \cdot N_{\text{INP, fogwater}} \quad (6)$$

Figure 9 depicts N_{INP} as determined from the clear-air filter samples with gray symbols and the ones derived from the fog water samples in yellow. Overall, measured and derived N_{INP} are in good agreement. Unfortunately, as multiple atmospheric filter samples were taken during the collection time of a single fog sample, an unambiguous attribution of a filter to a fog sample is difficult. Therefore, here we can only report the half-quantitative observation that the freezing spectra of the atmospheric filter samples taken concurrently with the most ice-active fog samples and the spectra derived from the fog water samples feature similar shapes, with the shapes themselves and the onset of freezing at temperatures above -10°C suggesting the presence of biogenic INPs. This clearly points at the same or at least similar, partly biogenic, INP populations being present in both fog droplets and atmospheric aerosol particles. Also Gong et al. (2020) found general agreement between N_{INP} in the air and N_{INP} derived from, in their case, cloud water samples. They further observed that highly ice-active particles are activated into cloud droplets during cloud events and then can be found in the cloud water. It is likely that a similar process occurs during our fog events.

It should be noted that if N_{CCN} changes significantly during the sampling time of the respective fog sample, the fog-derived atmospheric N_{INP} is directly affected. Such an instance can be seen in the lowest fog-derived INP spectra in Fig. 9, where the low average N_{CCN} led to a deviation of around 1 order of magnitude in comparison to the atmospheric sample. In the Supplement (Sect. S9), the fog-water-derived N_{INP} levels are shown for an extrapolated value of N_{CCN} at $\text{SS} = 0.02\%$. With that value, the agreement between the filter- and fog-derived N_{INP} is reduced; nevertheless, both still overlap by 1 to almost 2 orders of magnitude. A linear extrapolation to such low supersaturations has large uncertainties; hence, it should be only seen as an estimate for the lower boundary of the presented derivation method of N_{INP} in air from fog water samples.

3.4 Connecting atmospheric INPs to sea spray

In order to assess the ocean as a possible source of atmospheric INPs, we derive potential atmospheric N_{INP} by virtually dispersing the characterized seawater samples as sea spray (Irish et al., 2019b; Gong et al., 2020). This thought experiment can be paraphrased as follows: if the seawater samples including all their INPs would be directly dispersed into the air, scaled by the measured relation between salt in the air and in the water, what would be the resulting N_{INP} in the air?

For this approach, we use the amount of NaCl present in the atmospheric aerosol particles (derived from chemical analysis of Berner impactor samples) in relation to the

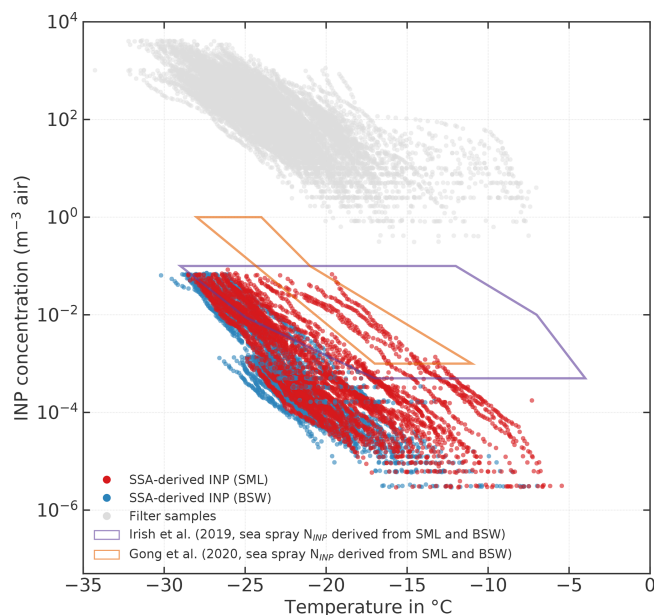


Figure 10. Sea-spray-derived atmospheric N_{INP} (red symbols = derived from SML samples; blue symbols = derived from BSW samples; measurements with INDA and LINA). The gray symbols show the filter-derived atmospheric N_{INP} . The orange and purple polygons indicate the range of sea spray aerosol (SSA)-derived N_{INP} by Irish et al. (2019b) and Gong et al. (2020), respectively. Samples from melt ponds are excluded.

amount of NaCl present in the seawater as a scaling factor to translate $N_{\text{INP}}^{\text{seawater}}$ into atmospheric N_{INP} . In this simple model, no enrichment of INPs is accounted for in the course of sea spray production. The sea-spray-derived INP concentrations ($N_{\text{INP}}^{\text{seaspray, air}}$) are calculated as

$$N_{\text{INP}}^{\text{seaspray, air}} = \frac{\text{NaCl}_{\text{mass, air}}}{\text{NaCl}_{\text{mass, seawater}}} \cdot N_{\text{INP}}^{\text{seawater}}, \quad (7)$$

where $\text{NaCl}_{\text{mass, air}}$ and $\text{NaCl}_{\text{seawater}}$ are the mass concentrations of sodium chloride in corresponding air and seawater samples, respectively. $\text{NaCl}_{\text{mass, air}}$ varied between 0.04 and $1.9 \mu\text{g m}^{-3}$ during the campaign with an average of $0.48 \mu\text{g m}^{-3}$. The average $\text{NaCl}_{\text{seawater}}$ of all SML and BSW samples is 32.5 g L^{-1} with actual concentrations varying between 25.7 and 34.5 g L^{-1} . $\text{NaCl}_{\text{seawater}}$ was derived from the salinity of the samples with the simplifying assumption that NaCl is the only salt in the sea water. This assumption is justified as non-NaCl salts represent only minor constituents of the sea water. Samples from melt ponds are excluded here and also in the following as they are mostly fresh water and therefore not suited for this approach that is based on NaCl concentration.

Figure 10 shows atmospheric filter-derived N_{INP} in gray and the sea-spray-derived $N_{\text{INP}}^{\text{seaspray, air}}$ (red symbols correspond to SML samples and blue ones to BSW samples). As can be seen, $N_{\text{INP}}^{\text{seaspray, air}}$ falls mostly in the range between

10^{-6} and 10^{-1} m^{-3} , which is approximately 3 to 5 orders of magnitude lower than the atmospheric N_{INP} derived from our atmospheric filter samples. Our lower end of the derived concentration range (10^{-6} m^{-3}) is also roughly 3 orders of magnitude lower than the lower end of the range reported by Gong et al. (2020), who sampled near the subtropical islands of Cabo Verde during late summer, and Irish et al. (2019b), who measured in the Canadian Arctic during early summer. These differences could be due to the geographical settings of the samples being vastly different, even for the Arctic measurements by Irish et al. (2019b). Irish et al. (2019b) took samples comparatively close to the shore mainly in the Nares Strait and Baffin Bay during summer with no extensive sea ice cover present, whereas we sampled mostly within the ice pack hundreds of nautical miles away from bigger lands masses. But even if the ranges given in Gong et al. (2020) and Irish et al. (2019b) are considered, our atmospheric filter-derived N_{INP} levels are still orders of magnitude higher than any sea-spray-derived N_{INP} . This indicates that sea spray aerosol as a sole source is not sufficient to explain atmospheric N_{INP} without significant enrichment of INPs during sea spray production. To the authors' knowledge, there are no studies available on the enrichment of INPs in sea spray aerosol (SSA). However, studies about the enrichment of bacteria and organic matter exist. Blanchard (1978) describes that in jet drops, which are produced when bubbles burst at the air–water interface, bacteria can get enriched by a factor greater than 10^3 . While several factors, including the type of bacteria themselves, control the EF of bacteria, the findings by Blanchard (1978) suggest that similar EFs may also apply to INP, since bacteria are a major contributor to seawater ice activity, as described in the introduction. For organic matter, EFs of 10^4 to 10^5 (in relation to mass) are reported for submicron SSA (Keene et al., 2007; Van Pinxteren et al., 2017) and 10^2 for supermicron SSA (Quinn et al., 2015; Keene et al., 2007). As we have no information about the size of the INPs, except that they are larger than $0.2 \mu\text{m}$, we cannot say what enrichment factor would be an appropriate assumption in regard to INPs, but the abovementioned literature indicates that processes exist that can produce sufficiently high enrichment factors at least for some substance classes. But it should be also noted that the laboratory study by Ickes et al. (2020) did not find a correlation between total organic carbon content of algal culture samples and the freezing of the sample. The same study confirmed that the transfer of ice-nucleating material from the seawater to the aerosol phase can indeed happen. Therefore, a marine source for the INPs in the Arctic atmosphere cannot be ruled out, but considerable enrichment of INPs during the transfer from the ocean surface to the atmosphere would have to take place.

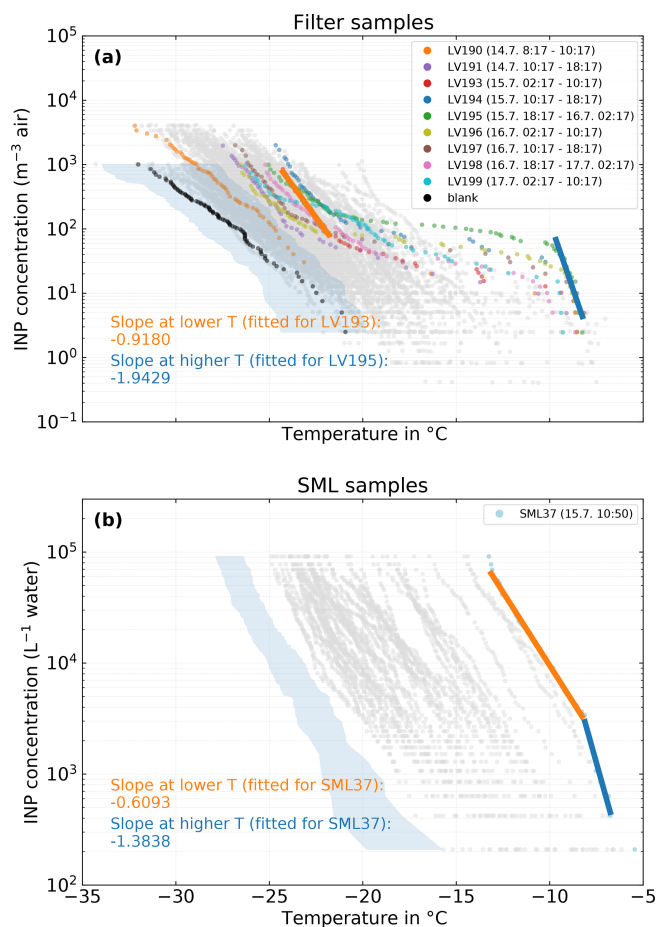


Figure 11. (a) Filter samples measured with LINA. Samples that were collected during the period of the case study are shown in color, while all other samples are shown in gray. Exemplary fits for the slopes at lower and higher temperatures for case-study-related samples are shown as orange and blue lines, respectively. The black dots depict the mean freezing spectrum of the field blanks scaled to atmospheric concentrations with the mean sampled air volume of the 8 h filter samples. (b) SML samples measured with INDA. The sample that was collected during the period of the case study is shown in color, while all other samples are shown in gray. As in (a), the fits of the slope are shown as orange and blue lines.

3.5 Case study

In Sect. 3.1, we described that INP concentrations are different in the ice-free ocean, within the ice pack, and close to land. In the following we will show that merely the proximity to land does not make marine INP sources inferior to terrestrial ones. To elucidate this, we consider a time period of several filter-sampling intervals which occurred around a time when both atmospheric and INP concentrations in the SML were highest. This happened close to Svalbard and in the vicinity of the ice edge, which makes the situation even more interesting.

The overall most ice-active SML sample, SML37, was taken on 15 July, 10:50 LT, and is highlighted in Fig. 11 (lower panel, light blue symbols). It occurs at the beginning of the sampling period of LV194, which is the second most ice-active atmospheric filter sample (Fig. 11, upper panel, blue symbols). A number of atmospheric samples collected before and after sample LV194 are also shown. Most of the $N_{\text{INP}}(T)$ spectra from these samples have a very similar overall shape, featuring a fairly steep increase at temperatures above -10°C , followed by a plateau region between ca. -10 and -21°C and another but less steep increase below -21°C . Such a behavior is indicative of the presence of distinct INP populations; therefore, not many mixing events happened during transport (Hartmann et al., 2020a; Welti et al., 2018). Additionally, the INPs active at these warmer temperatures are likely biogenic and proteinaceous as indicated by heat tests described in Sect. 3.1.

Temperature range and slope of, for example, the initial increase in the temperature spectra are somewhat characteristic for the INPs prevailing. In other words, similar slopes in similar temperature ranges observed for atmospheric and SML samples could be indicative of similar INPs being present in both compartments (Knackstedt et al., 2018). As shown in Fig. 11, the slope of the atmospheric samples at $T > -10^{\circ}\text{C}$ (linear fit on logarithmic axis) is -1.94 , while the slope of the SML sample at $T > -8.2^{\circ}\text{C}$ is -1.38 . The difference in these slopes is too large to unambiguously attribute both samples to the same INP species and too small to reject the possibility. In other words, the similarities in the spectra (temperature range and slopes) at the high freezing temperatures do not prove but can be taken as a hint at similar INPs being present in both the atmosphere and the SML. It is also apparent that the less steep slope at lower temperatures ($T < -8.2^{\circ}\text{C}$) of that SML sample has no counterpart in the atmospheric samples. If the atmospheric INPs active above -10°C would originate from the ocean, this suggests that the aerosolization process might be different for different INP species. Furthermore, it is possible that the INP flux is the other way around, i.e., INPs from the atmosphere are deposited into the SML. However this is highly speculative and needs further research.

To further elucidate the possible connection between atmospheric INPs and INPs in the SML, in the following we consider additionally available aerosol-related and meteorological information.

The highly ice-active sample discussed above, SML37, was taken during a period (approx. 14 July 18:00 to 15 July 19:30) which, as can be seen in Fig. 12, was characterized by a monomodal particle size distribution and, compared to the periods before and after, increased total particle number (N_{total} , panel b) and CCN (N_{CCN} , panel c) concentrations. In panel (d) it can be seen that during this period the wind speed decreased significantly, and the wind direction changed slowly from around 240 to 175° . Furthermore, during the collection times of the filter samples LV194 and

LV195, increased chlorophyll *a* concentrations were measured by the vessel's FerryBox system (panel e). The elevated chlorophyll *a* concentrations may indicate enhanced biological activity like a phytoplankton bloom in the vicinity of the vessel during the collection time of the samples LV194 and LV195. Interestingly the chlorophyll *a* concentration of the highly ice-active sample SML37 itself is not unusually high ($0.24\ \mu\text{g L}^{-1}$; Bracher, 2019). This may have two main reasons. Firstly, while chlorophyll *a* is an indicator for biological activity, not all marine microorganisms contain chlorophyll *a*. Secondly, since chlorophyll *a* itself is not the INP, a correlation is not necessarily to be expected. Also as described in Zeppenfeld et al. (2019) and the references within, the release of ice-active algal exudates may be a feature of decaying plankton blooms. Hence the peak in biological activity, indicated by the chlorophyll *a* concentration, may be already over, when the peak concentration of ice-active substances occurs. Lastly, panel (f) in Fig. 12 shows N_{INP} measured with SPIN. Similar to the filter-derived N_{INP} , also the INP measurements with SPIN remain fairly constant during the period of the case study, and no correlation with the other parameters shown in Fig. 12 can be seen.

To broaden the perspective beyond the aforementioned measurements at the position of the ship itself, HYSPLIT back-trajectories were also assessed.

In Fig. 13 the hourly 3 d back-trajectories (50 m arrival height) for the entire period depicted in Fig. 12 are shown. The color code indicates into which collection time, i.e., sample, the respective trajectories fall (corresponding to background colors used in Fig. 12). The trajectories can be categorized into four clusters. The first cluster consists of the trajectories belonging to the samples LV190 and LV191 (orange and purple). These trajectories travel mostly over the ice pack north of Svalbard and have no connection to land. The second cluster comprises the samples LV193, LV194, and LV195 (red, blue, and green), for which the air masses were at the east coast of Greenland before traveling along the ice edge and south of or over Svalbard, before reaching the ship. While CCN and INP number concentrations were elevated during the phase indicated by the red and blue trajectories, the phase connected to the green trajectory coincides with a strong lowering of CCN but still high INP concentrations. The third cluster, which consists of the samples LV197 and LV198 (yellow and brown), came from the same direction as the second cluster but made an additional loop towards the east and back, for which it took about 1 d. For these, N_{INP} were still high, with medium high concentrations of N_{CCN} and N_{tot} during the yellow phase. Unfortunately, aerosol characterization measurements were no longer continued after that time. The trajectories of the fourth cluster (LV198 and LV199; pink and cyan) come from the south and had contact with the Norwegian coast 1–2 d prior to their arrival at *Polarstern*. Additionally, Fig. S5 in the Supplement shows a map of the wider investigation area together with satellite measurements of chlorophyll *a* concentrations and

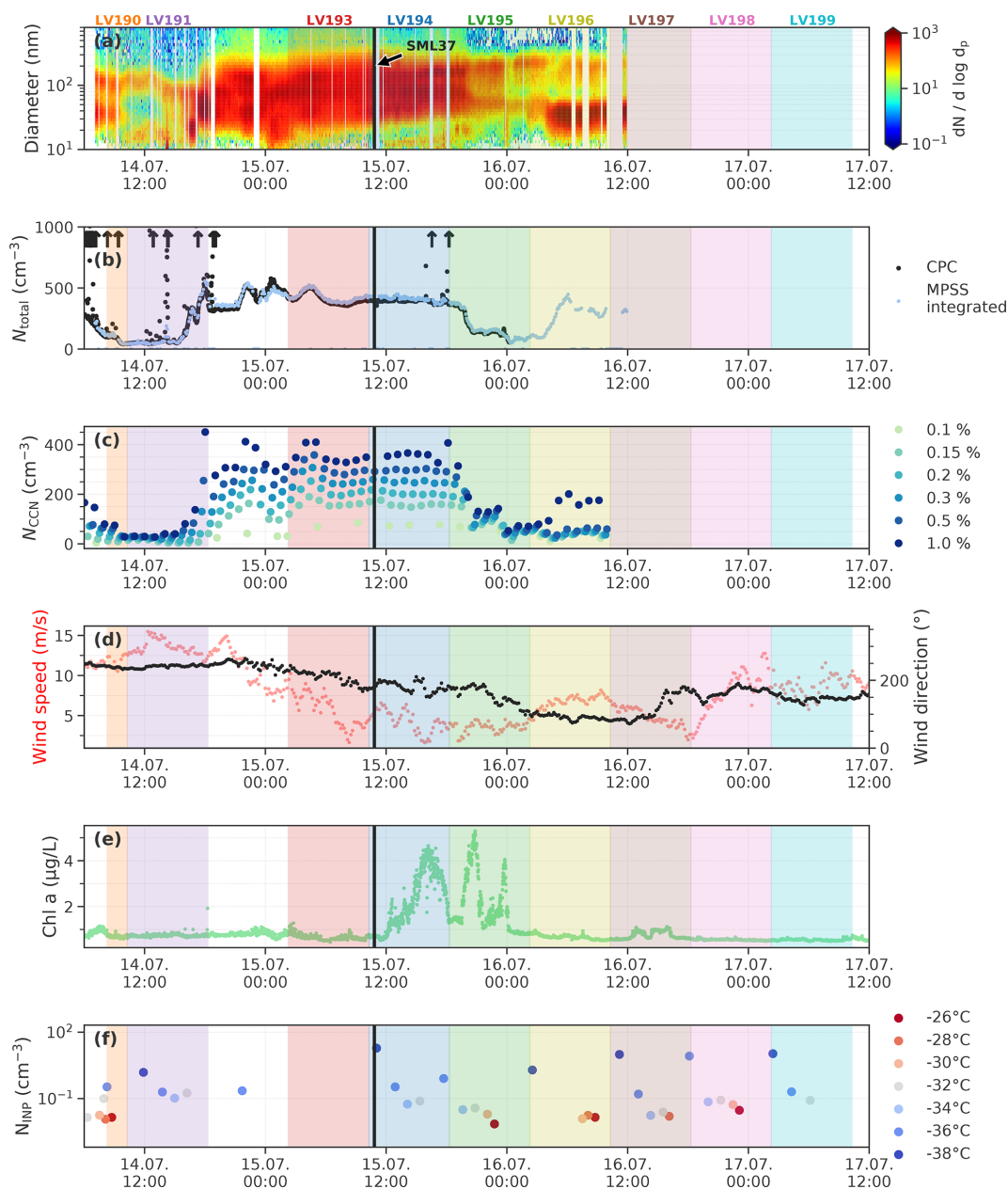


Figure 12. Aerosol measurements and other relevant parameters during the period of the case study. Shown are (a) the particle number size distribution, (b) the total particle concentrations N_{total} , (c) cloud concentration nuclei concentration (N_{CCN}) for 6 different supersaturations, (d) 10 min averages of wind direction and wind speed, (e) chlorophyll *a* concentration measured by the FerryBox system of *Polarstern*, and (f) the INP concentration (N_{INP}) measured with SPIN at different temperatures (color coded). The arrows in panel (b) indicate where total particle concentrations are higher than the axis limit. The colored shaded areas mark the periods where the filter samples were collected. The respective sample ID is shown on top. The black vertical line marks the collection time of the SML sample SML37.

the back-trajectories, where it can be seen that biological activity can be found in the region.

While it is a reasonable assumption that the INPs are produced in situ by biological processes, a recent publication by Cornwell et al. (2020) presents a different pathway. They show in a laboratory study that mineral dust deposited in seawater can be re-aerosolized and add to the atmospheric INP

population. This pathway is especially interesting as a pathway, because in proximity to the coast meltwater streams can transport dust into the ocean. Pfirman et al. (1989) also describe that sea ice often contains dust particles that can originate from atmospheric deposition or from shelf or shore-fast sea ice which may be transported away from the coast. And as Tobo et al. (2019) observed, dust can also be the carrier

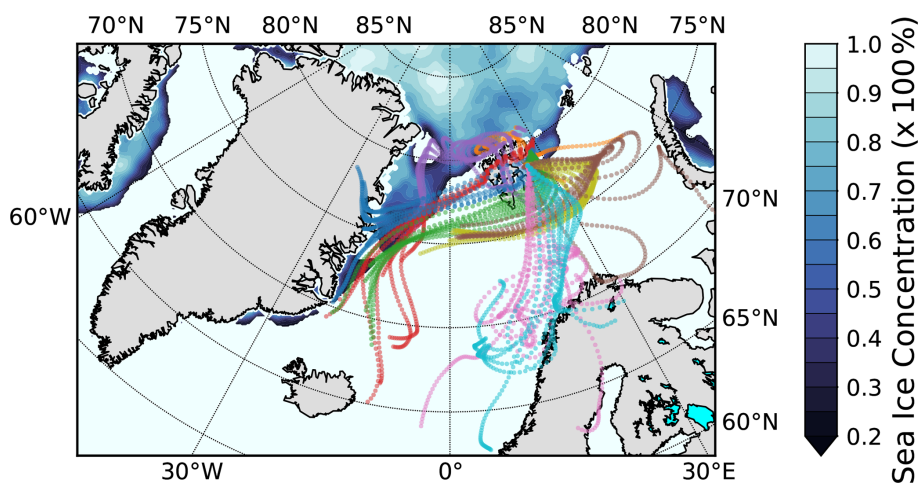


Figure 13. Hourly 3 d back-trajectories (50 m arrival height) for the collection time of the filter samples LV190 to LV199. The color code shows to which sample the trajectory belongs (consistent with Figs. 11 and 12). The Special Sensor Microwave Imager/Sounder (SSMIS) sea ice concentration with emphasized ice edge on 15 July 2017 is also shown (sea ice concentration product of the EUMETSAT Ocean and Sea Ice Satellite Application Facility).

for highly ice-active biogenic material; therefore, these dust-related processes may also explain spatially confined areas of high ice activity without being contradictory to the assumption of biogenic INP.

Summarizing and interpreting our observations, the following can be stated:

- The freezing spectra of atmospheric INPs are similar in shape, i.e., a steep slope at warm temperatures followed by an extended plateau region followed by less steep slope, indicating that during the case study similar atmospheric INP populations were sampled.
- Heat tests indicate that INPs active above -15°C are biogenic and proteinaceous.
- The freezing spectra of atmospheric INPs and INPs from the SML feature similar slopes at temperatures above -10°C , suggesting a connection between both compartments, which, however, as discussed above, would need a substantial enrichment of INPs during the sea spray production.
- Aerosol particle parameters show that clearly different air masses arrive at *Polarstern* over the course of the case study.
- Back-trajectories indicate that sampled air masses have different regions of origin and travel over different pathways towards *Polarstern*.
- Elevated chlorophyll *a* concentrations were observed for a short phase directly at the position of *Polarstern* (FerryBox) and also in the wider geographical region in the week-long satellite composite. This indicates a high biological activity in the investigation region.

We interpret these findings as strong indication for a local marine source being present during our case study. Seemingly this is in contradiction to the results gained from the analysis of fog water as presented above, unless a significant enrichment of INPs takes place during the aerosolization of seawater and/or SML material. In other words, there is a strong need for gaining knowledge concerning the mechanisms of aerosolization and resulting fluxes of INPs and related species at the ocean–atmosphere interface.

4 Summary and conclusions

We present the results of INP-related investigations carried out during a 2-month cruise (May–July 2017) on the RV *Polarstern* in the Arctic. Four different compartments, i.e., air, fog water, sea surface microlayer, and bulk seawater were sampled.

Concerning air sampling, throughout the whole cruise, 8 h filter samples for offline INP analysis in the TROPOS laboratories were taken, and a continuous-flow diffusion chamber provided online INP data. Fog samples were collected on an event basis, while samples from the SML and the bulk seawater were taken daily.

The time series of atmospheric N_{INP} derived from filters show that N_{INP} was low when the ship was located beyond the ice edge within the ice pack. Higher concentrations were observed outside the ice pack in the MIZ and the ice-free ocean. The highest INP concentrations occurred between both legs of the expedition, when *Polarstern* was near Longyearbyen harbor and when the vessel cruised along the MIZ at the eastern coast of the Svalbard archipelago at the end of the second leg. For most of the air samples, freezing was initiated below -15°C ; however, some samples featured

freezing onsets at warmer temperatures of up to -7°C . Heat tests suggest the presence of biogenic, proteinaceous INPs at temperatures above -15°C . At -32°C , the Arctic N_{INP} levels we observed are in the same order of magnitude as in the outflow region for mineral dust from the Sahara west of Africa, which indicates that at these low temperatures dust is an important INP even in the Arctic.

SML samples from the biologically active MIZ have a higher fraction of highly ice-active samples than the other ocean compartments (ice-free ocean, ice pack, melt pond). Besides that, the ice activity of SML and BSW samples is not simply correlated with the environment the sample was taken from. In general, few highly ice-active samples stand out against the other samples. Except for one case, we found the SML to be weakly to significantly enriched in INPs compared to the underlying BSW. The enrichment factors (EFs) varied between close to 1 and 94.97 at -15°C . The most enriched samples featured the highest ice activity in the SML samples.

From INP concentration in the fog water and the measured CCN number concentrations, we derived potential N_{INP} in the air, which we compared to the directly measured N_{INP} , and found good agreement. This indicates that the same, or at least similar, INP populations were present in corresponding fog water and air samples, suggesting that during fog events INPs are activated to droplets and become available as immersion nuclei inside the fog droplets.

Using the ratio of NaCl mass concentration in the air and in the seawater as a scaling factor, we assessed if atmospheric N_{INP} can be explained simply by aerosolization of SML and BSW material. At any given temperature we found SML- and BSW-derived N_{INP} to be 4 to 5 orders of magnitude lower than the N_{INP} directly measured in air. This clearly shows that aerosolization of SML or BSW material, without significant enrichment of INPs during aerosolization, does not suffice to explain N_{INP} in air. In other words, a marine source for the INPs in the Arctic atmosphere is possible, but enrichment of INPs by several orders of magnitude during the transfer from the ocean surface to the atmosphere has to take place. However, literature suggests that such EFs greater than 10^3 may be possible for INP.

In a case study we looked more deeply into a scenario for which coinciding SML and air samples were highly ice active. Thereby, we found similarities in the temperature spectra of the highly ice-active INPs in the SML and in the air. Air mass changes, indicated by changes in aerosol properties and back-trajectories, did not cause changes in the observed INP population. Isolated patches with chlorophyll *a* concentrations of about 1 order of magnitude higher compared to their surroundings underline high biological activity in the investigation region for the time period we investigated in the case study. We consider this as indications for a local biogenic marine source of INPs being present.

Altogether, we found INP concentrations in air, fog water, SML, and BSW to be highly variable, with a small number

of cases featuring significantly enhanced ice activity. This emphasizes the episodic, highly variable nature of INPs as was already described decades ago by Bigg (1961). This questions the appropriateness of parameterizations based on aerosol particle number in atmospheric models. We found indications for a marine biogenic INP source; however, further investigations are needed to gain quantitative knowledge concerning the aerosolization process and the resulting INP fluxes at the interface between the atmosphere and the ocean surface.

Lastly, to reply to the questions from the introduction, the following can be stated.

- *What is the abundance of Arctic INPs and in what temperature range can they nucleate ice?*

We found INPs active between -7 and -38°C over a concentration range from 4×10^{-1} to $1 \times 10^8 \text{ m}^{-3}$. Most of the time N_{INP} was at the lower end of the N_{INP} range known from midlatitudes or even lower. Exceptions were the upper and lower ends of the temperature range: at -10°C N_{INP} levels of up to $6 \times 10^1 \text{ m}^{-3}$ were observed, while at -32°C N_{INP} was in the same order of magnitude (10^5 m^{-3}) as in the outflow region of the Sahara.

- *What is the nature of Arctic INPs (biogenic material vs. mineral dust)?*

We find indications that the warmer temperatures ($> -15^{\circ}\text{C}$) are dominated by biogenic INP, while at colder temperatures ($< -25^{\circ}\text{C}$) mineral dust likely dominates.

- *What is the origin of Arctic INPs (local vs. long range transport, marine vs. terrestrial)?*

For the INPs at warmer temperatures, we find indications that they are marine and locally emitted, which, however, necessitates an enrichment of INPs during sea spray aerosol production of several orders of magnitude.

Data availability. Freezing spectra are made available at PANGAEA: <https://doi.org/10.1594/PANGAEA.919194> (Hartmann et al., 2020b).

Supplement. The supplement related to this article is available online at: <https://doi.org/10.5194/acp-21-11613-2021-supplement>.

Author contributions. MH analysed the data and wrote the paper with contributions from all co-authors; expedition preparation was conducted by all co-authors; MH, XG, and AnW conducted or assisted in the sample collection (filter, seawater, fog water) and performed the online measurements of CCN and INP; MvP and SZ conducted seawater sample collection, and SZ provided the salinity measurements of these samples. SK and TV conducted and provided the particle number size distribution and total particle concentration measurements. FS, AIW, and HH acquired the funding.

Competing interests. The authors declare that they have no conflict of interest.

Disclaimer. Publisher's note: Copernicus Publications remains neutral with regard to jurisdictional claims in published maps and institutional affiliations.

Special issue statement. This article is part of the special issue "Arctic mixed-phase clouds as studied during the ACLOUD/PASCAL campaigns in the framework of (AC)³ (ACP/AMT/ESSD inter-journal SI)". It is not associated with a conference.

Acknowledgements. We gratefully acknowledge the funding by the Deutsche Forschungsgemeinschaft (DFG, German Research Foundation) – project no. 268020496 – TRR 172, within the Transregional Collaborative Research Center "Arctic Amplification: Climate Relevant Atmospheric and SurfaCe Processes, and Feedback Mechanisms (AC)³". We thank Susanne Fuchs for the ion chromatographic measurements. We also thank Amelie Assenbaum, Audrey Brown, Mareike Löffler, and Jasmin Lubitz for their assistance with the cold-stage measurements.

Financial support. This research has been supported by the Deutsche Forschungsgemeinschaft (grant no. 268020496).

Review statement. This paper was edited by Amy Solomon and reviewed by Russell Schnell and two anonymous referees.

References

- Agresti, A. and Coull, B. A.: Approximate is Better than "Exact" for Interval Estimation of Binomial Proportions, *Am. Stat.*, 52, 119–126, <https://doi.org/10.1080/00031305.1998.10480550>, 1998.
- Alpert, P. A., Aller, J. Y., and Knopf, D. A.: Initiation of the ice phase by marine biogenic surfaces in supersaturated gas and supercooled aqueous phases, *Phys. Chem. Chem. Phys.*, 13, 19882–19894, <https://doi.org/10.1039/c1cp21844a>, 2011a.
- Alpert, P. A., Aller, J. Y., and Knopf, D. A.: Ice nucleation from aqueous NaCl droplets with and without marine diatoms, *Atmos. Chem. Phys.*, 11, 5539–5555, <https://doi.org/10.5194/acp-11-5539-2011>, 2011b.
- Arrigo, K. R., van Dijken, G., and Pabi, S.: Impact of a shrinking Arctic ice cover on marine primary production, *Geophys. Res. Lett.*, 35, 1–6, <https://doi.org/10.1029/2008GL035028>, 2008.
- Bierwirth, E., Ehrlich, A., Wendisch, M., Gayet, J.-F., Gourbeyre, C., Dupuy, R., Herber, A., Neuber, R., and Lampert, A.: Optical thickness and effective radius of Arctic boundary-layer clouds retrieved from airborne nadir and imaging spectrometry, *Atmos. Meas. Tech.*, 6, 1189–1200, <https://doi.org/10.5194/amt-6-1189-2013>, 2013.
- Bigg, E. K.: Natural Atmospheric Ice Nuclei, *Sci. Prog.*, 49, 458–475, 1961.
- Bigg, E. K.: Ice forming nuclei in the high Arctic, *Tellus B*, 48, 223–233, <https://doi.org/10.1034/j.1600-0889.1996.t01-1-00007.x>, 1996.
- Bigg, E. K. and Leck, C.: The composition of fragments of bubbles bursting at the ocean surface, *J. Geophys. Res.*, 113, D11209, <https://doi.org/10.1029/2007JD009078>, 2008.
- Blanchard, D. C.: Jet drop enrichment of bacteria, virus, and dissolved organic material, *Pure Appl. Geophys.*, 116, 302–308, <https://doi.org/10.1007/BF01636887>, 1978.
- Bracher, A.: Phytoplankton pigment concentration and phytoplankton groups measured on water samples obtained during POLARSTERN cruise PS106 in the Arctic Ocean, PANGAEA, <https://doi.org/10.1594/PANGAEA.899284>, 2019.
- Budke, C. and Koop, T.: BINARY: an optical freezing array for assessing temperature and time dependence of heterogeneous ice nucleation, *Atmos. Meas. Tech.*, 8, 689–703, <https://doi.org/10.5194/amt-8-689-2015>, 2015.
- Cohen, J., Zhang, X., Francis, J., Jung, T., Kwok, R., Overland, J., Ballinger, T. J., Bhatt, U. S., Chen, H. W., Coumou, D., Feldstein, S., Gu, H., Handorf, D., Henderson, G., Ionita, M., Kretschmer, M., Laliberte, F., Lee, S., Linderholm, H. W., Maslowski, W., Peings, Y., Pfeiffer, K., Rigor, I., Semmler, T., Stroeve, J., Taylor, P. C., Vavrus, S., Vihma, T., Wang, S., Wendisch, M., Wu, Y., and Yoon, J.: Divergent consensus on Arctic amplification influence on midlatitude severe winter weather, *Nat. Clim. Change*, 10, 20–29, <https://doi.org/10.1038/s41558-019-0662-y>, 2020.
- Conen, F. and Yakutin, M. V.: Soils rich in biological ice-nucleating particles abound in ice-nucleating macromolecules likely produced by fungi, *Biogeosciences*, 15, 4381–4385, <https://doi.org/10.5194/bg-15-4381-2018>, 2018.
- Conen, F., Morris, C. E., Leifeld, J., Yakutin, M. V., and Alewell, C.: Biological residues define the ice nucleation properties of soil dust, *Atmos. Chem. Phys.*, 11, 9643–9648, <https://doi.org/10.5194/acp-11-9643-2011>, 2011.
- Conen, F., Henne, S., Morris, C. E., and Alewell, C.: Atmospheric ice nucleators active $\geq -12^\circ\text{C}$ can be quantified on PM₁₀ filters, *Atmos. Meas. Tech.*, 5, 321–327, <https://doi.org/10.5194/amt-5-321-2012>, 2012.
- Conen, F., Eckhardt, S., Gundersen, H., Stohl, A., and Yttri, K. E.: Rainfall drives atmospheric ice-nucleating particles in the coastal climate of southern Norway, *Atmos. Chem. Phys.*, 17, 11065–11073, <https://doi.org/10.5194/acp-17-11065-2017>, 2017.
- Cornwell, G. C., Sultana, C. M., Prank, M., Cochran, R. E., Hill, T. C. J., Schill, G. P., DeMott, P. J., Mahowald, N., and Prather, K. A.: Ejection of dust from the ocean as a potential source of marine ice nucleating particles, *J. Geophys. Res.-Atmos.*, 25, e2020JD033073, <https://doi.org/10.1029/2020JD033073>, 2020.
- Costa, A., Meyer, J., Afchine, A., Luebke, A., Günther, G., Dorsey, J. R., Gallagher, M. W., Ehrlich, A., Wendisch, M., Baumgardner, D., Wex, H., and Krämer, M.: Classification of Arctic, midlatitude and tropical clouds in the mixed-phase temperature regime, *Atmos. Chem. Phys.*, 17, 12219–12238, <https://doi.org/10.5194/acp-17-12219-2017>, 2017.
- Creamean, J. M., Kirpes, R. M., Pratt, K. A., Spada, N. J., Maahn, M., de Boer, G., Schnell, R. C., and China, S.: Marine and terrestrial influences on ice nucleating particles during continuous springtime measurements in an Arctic oilfield location, *Atmos.*

- Chem. Phys., 18, 18023–18042, <https://doi.org/10.5194/acp-18-18023-2018>, 2018.
- Creamean, J. M., Cross, J. N., Pickart, R., McRaven, L., Lin, P., Pacini, A., Hanlon, R., Schmale, D. G., Cenicerros, J., Aydele, T., Colombi, N., Bolger, E., and DeMott, P. J.: Ice Nucleating Particles Carried From Below a Phytoplankton Bloom to the Arctic Atmosphere, *Geophys. Res. Lett.*, 46, 2019GL083039, <https://doi.org/10.1029/2019GL083039>, 2019.
- Creamean, J. M., Hill, T. C. J., DeMott, P. J., Uetake, J., Kreidenweis, S., and Douglas, T. A.: Thawing permafrost: an overlooked source of seeds for Arctic cloud formation, *Environ. Res. Lett.*, 15, 084022, <https://doi.org/10.1088/1748-9326/ab87d3>, 2020.
- Demoz, B., Collett, J., and Daube, B.: On the Caltech Active Strand Cloudwater Collectors, *Atmos. Res.*, 41, 47–62, [https://doi.org/10.1016/0169-8095\(95\)00044-5](https://doi.org/10.1016/0169-8095(95)00044-5), 1996.
- Engel, A., Bange, H. W., Cunliffe, M., Burrows, S. M., Friedrichs, G., Galgani, L., Herrmann, H., Hertkorn, N., Johnson, M., Liss, P. S., Quinn, P. K., Schartau, M., Soloviev, A., Stolle, C., Upstill-Goddard, R. C., van Pinxteren, M., and Zäncker, B.: The Ocean's Vital Skin: Toward an Integrated Understanding of the Sea Surface Microlayer, *Front. Mar. Sci.*, 4, 165, <https://doi.org/10.3389/fmars.2017.00165>, 2017.
- Felgitsch, L., Baloh, P., Burkart, J., Mayr, M., Momken, M. E., Seifried, T. M., Winkler, P., Schmale III, D. G., and Grothe, H.: Birch leaves and branches as a source of ice-nucleating macromolecules, *Atmos. Chem. Phys.*, 18, 16063–16079, <https://doi.org/10.5194/acp-18-16063-2018>, 2018.
- Garimella, S., Kristensen, T. B., Ignatius, K., Welti, A., Voigtländer, J., Kulkarni, G. R., Sagan, F., Kok, G. L., Dorsey, J., Nichman, L., Rothenberg, D. A., Rösch, M., Kirchgäßner, A. C. R., Ladkin, R., Wex, H., Wilson, T. W., Ladino, L. A., Abbatt, J. P. D., Stetzer, O., Lohmann, U., Stratmann, F., and Cziczko, D. J.: The SPectrometer for Ice Nuclei (SPIN): an instrument to investigate ice nucleation, *Atmos. Meas. Tech.*, 9, 2781–2795, <https://doi.org/10.5194/amt-9-2781-2016>, 2016.
- Gong, X., Wex, H., van Pinxteren, M., Triesch, N., Fomba, K. W., Lubitz, J., Stolle, C., Robinson, T.-B., Müller, T., Herrmann, H., and Stratmann, F.: Characterization of aerosol particles at Cabo Verde close to sea level and at the cloud level – Part 2: Ice-nucleating particles in air, cloud and seawater, *Atmos. Chem. Phys.*, 20, 1451–1468, <https://doi.org/10.5194/acp-20-1451-2020>, 2020.
- Groot Zwaafink, C. D., Grythe, H., Skov, H., and Stohl, A.: Substantial contribution of northern high-latitude sources to mineral dust in the Arctic, *J. Geophys. Res.-Atmos.*, 121, 13678–13697, <https://doi.org/10.1002/2016JD025482>, 2016.
- Gysel, M. and Stratmann, F.: WP3- NA3: In-situ chemical, physical and optical properties of aerosols Deliverable D3.11: Standardized protocol for CCN measurements, Tech. rep., ACTRIS, available at: <https://actris-ecac.eu/ccn-nc.html#pdf-2> (last access: 20 July 2021), 2013.
- Hara, K., Maki, T., Kakikawa, M., Kobayashi, F., and Matsuki, A.: Effects of different temperature treatments on biological ice nuclei in snow samples, *Atmos. Environ.*, 140, 415–419, <https://doi.org/10.1016/j.atmosenv.2016.06.011>, 2016.
- Hartmann, M., Blunier, T., Brügger, S., Schmale, J., Schwikowski, M., Vogel, A., Wex, H., and Stratmann, F.: Variation of Ice Nucleating Particles in the European Arctic Over the Last Centuries, *Geophys. Res. Lett.*, 46, 2019GL082311, <https://doi.org/10.1029/2019GL082311>, 2019.
- Hartmann, M., Adachi, K., Eppers, O., Haas, C., Herber, A., Holzinger, R., Hünerbein, A., Jäkel, E., Jentsch, C., van Pinxteren, M., Wex, H., Willmes, S., and Stratmann, F.: Wintertime Airborne Measurements of Ice Nucleating Particles in the High Arctic: A Hint to a Marine, Biogenic Source for Ice Nucleating Particles, *Geophys. Res. Lett.*, 47, e2020GL087770, <https://doi.org/10.1029/2020GL087770>, 2020a.
- Hartmann, M., Gong, X., Welti, A., and Stratmann, F.: Shipborne Ice Nucleating Particle (INP) measurements in the Arctic during PS106.1 and PS106.2, Leibniz-Institut für Troposphärenforschung e.V., Leipzig, PANGAEA, <https://doi.org/10.1594/PANGAEA.919194>, 2020b.
- Hill, T. C. J., DeMott, P. J., Tobo, Y., Fröhlich-Nowoisky, J., Mofkett, B. F., Franc, G. D., and Kreidenweis, S. M.: Sources of organic ice nucleating particles in soils, *Atmos. Chem. Phys.*, 16, 7195–7211, <https://doi.org/10.5194/acp-16-7195-2016>, 2016.
- Hinzman, L. D., Bettez, N. D., Bolton, W. R., Chapin, F. S., Dyurgerov, M. B., Fastie, C. L., Griffith, B., Hollister, R. D., Hope, A., Huntington, H. P., Jensen, A. M., Jia, G. J., Jorgenson, T., Kane, D. L., Klein, D. R., Kofinas, G., Lynch, A. H., Lloyd, A. H., McGuire, A. D., Nelson, F. E., Oechel, W. C., Osterkamp, T. E., Racine, C. H., Romanovsky, V. E., Stone, R. S., Stow, D. A., Sturm, M., Tweedie, C. E., Vourlitis, G. L., Walker, M. D., Walker, D. A., Webber, P. J., Welker, J. M., Winker, K. S., and Yoshikawa, K.: Evidence and Implications of Recent Climate Change in Northern Alaska and Other Arctic Regions, *Climatic Change*, 72, 251–298, <https://doi.org/10.1007/s10584-005-5352-2>, 2005.
- Huang, S., Hu, W., Chen, J., Wu, Z., Zhang, D., and Fu, P.: Overview of biological ice nucleating particles in the atmosphere, *Environ. Int.*, 146, 106197, <https://doi.org/10.1016/j.envint.2020.106197>, 2021.
- Ickes, L., Porter, G. C. E., Wagner, R., Adams, M. P., Bierbauer, S., Bertram, A. K., Bilde, M., Christiansen, S., Ekman, A. M. L., Gorokhova, E., Höhler, K., Kiselev, A. A., Leck, C., Möhler, O., Murray, B. J., Schiebel, T., Ullrich, R., and Salter, M. E.: The ice-nucleating activity of Arctic sea surface microlayer samples and marine algal cultures, *Atmos. Chem. Phys.*, 20, 11089–11117, <https://doi.org/10.5194/acp-20-11089-2020>, 2020.
- Intrieri, J. M.: An annual cycle of Arctic surface cloud forcing at SHEBA, *J. Geophys. Res.*, 107, 8039, <https://doi.org/10.1029/2000JC000439>, 2002.
- Irish, V. E., Elizondo, P., Chen, J., Chou, C., Charette, J., Lizotte, M., Ladino, L. A., Wilson, T. W., Gosselin, M., Murray, B. J., Polishchuk, E., Abbatt, J. P. D., Miller, L. A., and Bertram, A. K.: Ice-nucleating particles in Canadian Arctic sea-surface microlayer and bulk seawater, *Atmos. Chem. Phys.*, 17, 10583–10595, <https://doi.org/10.5194/acp-17-10583-2017>, 2017.
- Irish, V. E., Hanna, S. J., Willis, M. D., China, S., Thomas, J. L., Wentzell, J. J. B., Cirisan, A., Si, M., Leaitch, W. R., Murphy, J. G., Abbatt, J. P. D., Laskin, A., Girard, E., and Bertram, A. K.: Ice nucleating particles in the marine boundary layer in the Canadian Arctic during summer 2014, *Atmos. Chem. Phys.*, 19, 1027–1039, <https://doi.org/10.5194/acp-19-1027-2019>, 2019a.
- Irish, V. E., Hanna, S. J., Xi, Y., Boyer, M., Polishchuk, E., Ahmed, M., Chen, J., Abbatt, J. P. D., Gosselin, M., Chang, R., Miller, L. A., and Bertram, A. K.: Revisiting properties and concen-

- trations of ice-nucleating particles in the sea surface microlayer and bulk seawater in the Canadian Arctic during summer, *Atmos. Chem. Phys.*, 19, 7775–7787, <https://doi.org/10.5194/acp-19-7775-2019>, 2019b.
- Joly, M., Amato, P., Deguillaume, L., Monier, M., Hoose, C., and Delort, A.-M.: Quantification of ice nuclei active at near 0 °C temperatures in low-altitude clouds at the Puy de Dôme atmospheric station, *Atmos. Chem. Phys.*, 14, 8185–8195, <https://doi.org/10.5194/acp-14-8185-2014>, 2014.
- Kecorius, S., Vogl, T., Paasonen, P., Lampilahti, J., Rothenberg, D., Wex, H., Zeppenfeld, S., van Pinxteren, M., Hartmann, M., Henning, S., Gong, X., Welti, A., Kulmala, M., Stratmann, F., Herrmann, H., and Wiedensohler, A.: New particle formation and its effect on cloud condensation nuclei abundance in the summer Arctic: a case study in the Fram Strait and Barents Sea, *Atmos. Chem. Phys.*, 19, 14339–14364, <https://doi.org/10.5194/acp-19-14339-2019>, 2019.
- Keene, W. C., Maring, H., Maben, J. R., Kieber, D. J., Pszenny, A. A. P., Dahl, E. E., Izaguirre, M. A., Davis, A. J., Long, M. S., Zhou, X., Smoydzin, L., and Sander, R.: Chemical and physical characteristics of nascent aerosols produced by bursting bubbles at a model air-sea interface, *J. Geophys. Res.-Atmos.*, 112, D21202, <https://doi.org/10.1029/2007JD008464>, 2007.
- King, M. D., Platnick, S., Yang, P., Arnold, G. T., Gray, M. A., Riedi, J. C., Ackerman, S. A., and Liou, K.-N.: Remote Sensing of Liquid Water and Ice Cloud Optical Thickness and Effective Radius in the Arctic: Application of Airborne Multispectral MAS Data, *J. Atmos. Ocean. Tech.*, 21, 857–875, [https://doi.org/10.1175/1520-0426\(2004\)021<0857:RSOLWA>2.0.CO;2](https://doi.org/10.1175/1520-0426(2004)021<0857:RSOLWA>2.0.CO;2), 2004.
- Kirpes, R. M., Bonanno, D., May, N. W., Fraund, M., Barget, A. J., Moffet, R. C., Ault, A. P., and Pratt, K. A.: Wintertime Arctic Sea Spray Aerosol Composition Controlled by Sea Ice Lead Microbiology, *ACS Central Science*, 5, 1760–1767, <https://doi.org/10.1021/acscentsci.9b00541>, 2019.
- Knackstedt, K. A., Moffett, B. F., Hartmann, S., Wex, H., Hill, T. C. J., Glasgo, E. D., Reitz, L. A., Augustin-Bauditz, S., Beall, B. F. N., Bullerjahn, G. S., Fröhlich-Nowoisky, J., Grawe, S., Lubitz, J., Stratmann, F., and McKay, R. M. L.: Terrestrial Origin for Abundant Riverine Nanoscale Ice-Nucleating Particles, *Environ. Sci. Technol.*, 52, 12358–12367, <https://doi.org/10.1021/acs.est.8b03881>, 2018.
- Knopf, D. A., Alpert, P. A., Wang, B., and Aller, J. Y.: Stimulation of ice nucleation by marine diatoms, *Nat. Geosci.*, 4, 88–90, <https://doi.org/10.1038/ngeo1037>, 2011.
- Knust, R.: Polar research and supply vessel POLARSTERN operated by the Alfred-Wegener-Institute, *Journal of large-scale research facilities JLSRF*, 3, A119, <https://doi.org/10.17815/jlsrf-3-163>, 2017.
- Koop, T. and Zobrist, B.: Parameterizations for ice nucleation in biological and atmospheric systems, *Phys. Chem. Chem. Phys.*, 11, 10839–10850, <https://doi.org/10.1039/B914289D>, 2009.
- Kunert, A. T., Pöhlker, M. L., Tang, K., Krevert, C. S., Wieder, C., Speth, K. R., Hanson, L. E., Morris, C. E., Schmale III, D. G., Pöschl, U., and Fröhlich-Nowoisky, J.: Macromolecular fungal ice nuclei in *Fusarium*: effects of physical and chemical processing, *Biogeosciences*, 16, 4647–4659, <https://doi.org/10.5194/bg-16-4647-2019>, 2019.
- Kuznetsova, M. and Lee, C.: Dissolved free and combined amino acids in nearshore seawater, sea surface microlayers and foams: Influence of extracellular hydrolysis, *Aquat. Sci.*, 64, 252–268, <https://doi.org/10.1007/s00027-002-8070-0>, 2002.
- Kwok, R., Cunningham, G. F., Wensnahan, M., Rigor, I., Zwally, H. J., and Yi, D.: Thinning and volume loss of the Arctic Ocean sea ice cover: 2003–2008, *J. Geophys. Res.*, 114, C07005, <https://doi.org/10.1029/2009JC005312>, 2009.
- Lang, A., Yang, S., and Kaas, E.: Sea ice thickness and recent Arctic warming, *Geophys. Res. Lett.*, 44, 409–418, <https://doi.org/10.1002/2016GL071274>, 2017.
- Leck, C. and Bigg, E. K.: Biogenic particles in the surface microlayer and overlying atmosphere in the central Arctic Ocean during summer, *Tellus B*, 57, 305–316, <https://doi.org/10.3402/tellusb.v57i4.16546>, 2005.
- Liu, Y. and Key, J. R.: Less winter cloud aids summer 2013 Arctic sea ice return from 2012 minimum, *Environ. Res. Lett.*, 9, 044002, <https://doi.org/10.1088/1748-9326/9/4/044002>, 2014.
- Loewe, K., Ekman, A. M. L., Paukert, M., Sedlar, J., Tjernström, M., and Hoose, C.: Modelling micro- and macrophysical contributors to the dissipation of an Arctic mixed-phase cloud during the Arctic Summer Cloud Ocean Study (ASCOS), *Atmos. Chem. Phys.*, 17, 6693–6704, <https://doi.org/10.5194/acp-17-6693-2017>, 2017.
- Macke, A. and Flores, H.: The Expeditions PS106/1 and 2 of the Research Vessel POLARSTERN to the Arctic Ocean in 2017, *Berichte zur Polar- und Meeresforschung (Reports on polar and marine research)*, 719, 1–171, https://doi.org/10.2312/BzPM_0719_2018, 2018.
- McCluskey, C. S., Hill, T. C. J., Humphries, R. S., Rauker, A. M., Moreau, S., Strutton, P. G., Chambers, S. D., Williams, A. G., McRobert, I., Ward, J., Keywood, M. D., Harnwell, J., Ponsonby, W., Loh, Z. M., Krummel, P. B., Protat, A., Kreidenweis, S. M., and DeMott, P. J.: Observations of Ice Nucleating Particles Over Southern Ocean Waters, *Geophys. Res. Lett.*, 45, 11989–11997, <https://doi.org/10.1029/2018GL079981>, 2018a.
- McCluskey, C. S., Hill, T. C. J., Sultana, C. M., Laskina, O., Trueblood, J., Santander, M. V., Beall, C. M., Michaud, J., Kreidenweis, S. M., Prather, K. A., Grassian, V., and DeMott, P. J.: A Mesocosm Double Feature: Insights into the Chemical Makeup of Marine Ice Nucleating Particles, *J. Atmos. Sci.*, 75, 2405–2423, <https://doi.org/10.1175/JAS-D-17-0155.1>, 2018b.
- Moffett, B. F., Hill, T. C. J., and DeMott, P. J.: Abundance of Biological Ice Nucleating Particles in the Mississippi and Its Major Tributaries, *Atmosphere*, 9, 307, <https://doi.org/10.3390/atmos9080307>, 2018.
- Müller, K., Lehmann, S., van Pinxteren, D., Gnauk, T., Niedermeier, N., Wiedensohler, A., and Herrmann, H.: Particle characterization at the Cape Verde atmospheric observatory during the 2007 RHaMBLe intensive, *Atmos. Chem. Phys.*, 10, 2709–2721, <https://doi.org/10.5194/acp-10-2709-2010>, 2010.
- Murray, B. J., O’Sullivan, D., Atkinson, J. D., and Webb, M. E.: Ice nucleation by particles immersed in supercooled cloud droplets, *Chem. Soc. Rev.*, 41, 6519, <https://doi.org/10.1039/c2cs35200a>, 2012.
- O’Sullivan, D., Adams, M. P., Tarn, M. D., Harrison, A. D., Vergara-Temprado, J., Porter, G. C. E., Holden, M. A., Sanchez-Marroquin, A., Carotenuto, F., Whale, T. F., McQuaid, J. B., Walshaw, R., Hedges, D. H. P., Burke, I. T., Cui, Z., and Mur-

- ray, B. J.: Contributions of biogenic material to the atmospheric ice-nucleating particle population in North Western Europe, *Sci. Rep.*, 8, 13821, <https://doi.org/10.1038/s41598-018-31981-7>, 2018.
- Ovchinnikov, M., Ackerman, A. S., Avramov, A., Cheng, A., Fan, J., Fridlind, A. M., Ghan, S., Harrington, J., Hoose, C., Korolev, A., McFarquhar, G. M., Morrison, H., Paukert, M., Savre, J., Shipway, B. J., Shupe, M. D., Solomon, A., and Sulia, K.: Intercomparison of large-eddy simulations of Arctic mixed-phase clouds: Importance of ice size distribution assumptions, *J. Adv. Model. Earth Sy.*, 6, 223–248, <https://doi.org/10.1002/2013MS000282>, 2014.
- Overland, J. E., Wood, K. R., and Wang, M.: Warm Arctic-cold continents: Climate impacts of the newly open arctic sea, *Polar Res.*, 30, 15787, <https://doi.org/10.3402/polar.v30i0.15787>, 2011.
- Park, H.-S., Lee, S., Kosaka, Y., Son, S.-W., and Kim, S.-W.: The Impact of Arctic Winter Infrared Radiation on Early Summer Sea Ice, *J. Climate*, 28, 6281–6296, <https://doi.org/10.1175/JCLI-D-14-00773.1>, 2015.
- Petersen, W., Colijn, F., Hydes, D., and Schroeder, F.: FerryBox: from on-line oceanographic observations to environmental information, EU Project FerryBox 2002–2005, EuroGOOS, Amsterdam, The Netherlands, 2007.
- Petersen, W., Schroeder, F., and Bockelmann, F.-D.: FerryBox – Application of continuous water quality observations along transects in the North Sea, *Ocean Dynam.*, 61, 1541–1554, <https://doi.org/10.1007/s10236-011-0445-0>, 2011.
- Petters, M. D. and Wright, T. P.: Revisiting ice nucleation from precipitation samples, *Geophys. Res. Lett.*, 42, 8758–8766, <https://doi.org/10.1002/2015GL065733>, 2015.
- Pfeifer, S., Birmili, W., Schladitz, A., Müller, T., Nowak, A., and Wiedensohler, A.: A fast and easy-to-implement inversion algorithm for mobility particle size spectrometers considering particle number size distribution information outside of the detection range, *Atmos. Meas. Tech.*, 7, 95–105, <https://doi.org/10.5194/amt-7-95-2014>, 2014.
- Pfirman, S., Wollenburg, I., Thiede, J., and Lange, M. A.: Lithogenic sediment on Arctic pack ice: Potential aeolian flux and contribution to deep sea sediments, in: *Paleoclimatology and paleometeorology: modern and past patterns of global atmospheric transport*, 463–493, Springer, Dordrecht, The Netherlands, 1989.
- Pinto, J. O.: Autumnal Mixed-Phase Cloudy Boundary Layers in the Arctic, *J. Atmos. Sci.*, 55, 2016–2038, [https://doi.org/10.1175/1520-0469\(1998\)055<2016:AMPCBL>2.0.CO;2](https://doi.org/10.1175/1520-0469(1998)055<2016:AMPCBL>2.0.CO;2), 1998.
- Pithan, F. and Mauritsen, T.: Arctic amplification dominated by temperature feedbacks in contemporary climate models, *Nat. Geosci.*, 7, 181–184, <https://doi.org/10.1038/ngeo2071>, 2014.
- Pouleur, S., Richard, C., Martin, J.-G., and Antoun, H.: Ice Nucleation Activity in *Fusarium acuminatum* and *Fusarium avenaceum*, *Appl. Environ. Microb.*, 58, 2960–2964, 1992.
- Prenni, A. J., DeMott, P. J., Kreidenweis, S. M., Harrington, J. Y., Avramov, A., Verlinde, J., Tjernström, M., Long, C. N., and Olsson, P. Q.: Can Ice-Nucleating Aerosols Affect Arctic Seasonal Climate?, *B. Am. Meteorol. Soc.*, 88, 541–550, <https://doi.org/10.1175/BAMS-88-4-541>, 2007.
- Pruppacher, H. and Klett, J.: *Microphysics of Clouds and Precipitation*, Atmospheric and Oceanographic Sciences Library, Springer Netherlands, Dordrecht, 2 edn., <https://doi.org/10.1007/978-0-306-48100-0>, 2010.
- Quinn, P. K., Collins, D. B., Grassian, V. H., Prather, K. A., and Bates, T. S.: Chemistry and Related Properties of Freshly Emitted Sea Spray Aerosol, *Chem. Rev.*, 115, 4383–4399, <https://doi.org/10.1021/cr500713g>, 2015.
- Roberts, G. C. and Nenes, A.: A Continuous-Flow Streamwise Thermal-Gradient CCN Chamber for Atmospheric Measurements, *Aerosol. Sci. Tech.*, 39, 206–221, <https://doi.org/10.1080/027868290913988>, 2005.
- Rolph, G., Stein, A., and Stunder, B.: Real-time Environmental Applications and Display sYstem: READY, *Environ. Modell. Softw.*, 95, 210–228, <https://doi.org/10.1016/j.envsoft.2017.06.025>, 2017.
- Sanchez-Marroquin, A., Arnalds, O., Baustian-Dorsi, K. J., Browse, J., Dagsson-Waldhauserova, P., Harrison, A. D., Maters, E. C., Pringle, K. J., Vergara-Temprado, J., Burke, I. T., McQuaid, J. B., Carslaw, K. S., and Murray, B. J.: Iceland is an episodic source of atmospheric ice-nucleating particles relevant for mixed-phase clouds, *Sci. Adv.*, 6, eaba8137, <https://doi.org/10.1126/sciadv.aba8137>, 2020.
- Šantl-Temkiv, T., Lange, R., Beddows, D. C., Rauter, U., Pilgaard, S., Dall’Osto, M., Gunde-Cimerman, N., Massling, A., and Wex, H.: Biogenic Sources of Ice Nucleation Particles at the High Arctic Site Villum Research Station, *Environ. Sci. Technol.*, 53, 10580–10590, <https://doi.org/10.1021/acs.est.9b00991>, 2019.
- Schnell, R. C.: Ice Nuclei in Seawater, Fog Water and Marine Air off the Coast of Nova Scotia: Summer 1975, *J. Atmos. Sci.*, 34, 1299–1305, [https://doi.org/10.1175/1520-0469\(1977\)034<1299:INISFW>2.0.CO;2](https://doi.org/10.1175/1520-0469(1977)034<1299:INISFW>2.0.CO;2), 1977.
- Schnell, R. C. and Vali, G.: Biogenic Ice Nuclei: Part I. Terrestrial and Marine Sources, *J. Atmos. Sci.*, 33, 1554–1564, [https://doi.org/10.1175/1520-0469\(1976\)033<1554:BINPIT>2.0.CO;2](https://doi.org/10.1175/1520-0469(1976)033<1554:BINPIT>2.0.CO;2), 1976.
- Serreze, M. C. and Barry, R. G.: Processes and impacts of Arctic amplification: A research synthesis, *Global Planet. Change*, 77, 85–96, <https://doi.org/10.1016/j.gloplacha.2011.03.004>, 2011.
- Shupe, M. D. and Intrieri, J. M.: Cloud Radiative Forcing of the Arctic Surface: The Influence of Cloud Properties, Surface Albedo, and Solar Zenith Angle, *J. Climate*, 17, 616–628, [https://doi.org/10.1175/1520-0442\(2004\)017<0616:CRFOTA>2.0.CO;2](https://doi.org/10.1175/1520-0442(2004)017<0616:CRFOTA>2.0.CO;2), 2004.
- Shupe, M. D., Uttal, T., Matrosov, S. Y., and Frisch, A. S.: Cloud water contents and hydrometeor sizes during the FIRE Arctic Clouds Experiment, *J. Geophys. Res.-Atmos.*, 106, 15015–15028, <https://doi.org/10.1029/2000JD900476>, 2001.
- Shupe, M. D., Matrosov, S. Y., and Uttal, T.: Arctic Mixed-Phase Cloud Properties Derived from Surface-Based Sensors at SHEBA, *J. Atmos. Sci.*, 63, 697–711, <https://doi.org/10.1175/JAS3659.1>, 2006.
- Shupe, M. D., Walden, V. P., Eloranta, E., Uttal, T., Campbell, J. R., Starkweather, S. M., and Shiobara, M.: Clouds at Arctic Atmospheric Observatories. Part I: Occurrence and Macrophysical Properties, *J. Appl. Meteorol. Clim.*, 50, 626–644, <https://doi.org/10.1175/2010JAMC2467.1>, 2011.
- Solomon, A., Feingold, G., and Shupe, M. D.: The role of ice nuclei recycling in the maintenance of cloud ice in Arctic mixed-phase stratocumulus, *Atmos. Chem. Phys.*, 15, 10631–10643, <https://doi.org/10.5194/acp-15-10631-2015>, 2015.

- Solomon, A., de Boer, G., Creamean, J. M., McComiskey, A., Shupe, M. D., Maahn, M., and Cox, C.: The relative impact of cloud condensation nuclei and ice nucleating particle concentrations on phase partitioning in Arctic mixed-phase stratocumulus clouds, *Atmos. Chem. Phys.*, 18, 17047–17059, <https://doi.org/10.5194/acp-18-17047-2018>, 2018.
- Stein, A. F., Draxler, R. R., Rolph, G. D., Stunder, B. J. B., Cohen, M. D., and Ngan, F.: NOAA's HYSPLIT Atmospheric Transport and Dispersion Modeling System, *B. Am. Meteorol. Soc.*, 96, 2059–2077, <https://doi.org/10.1175/BAMS-D-14-00110.1>, 2015.
- Tobo, Y., Adachi, K., DeMott, P. J., Hill, T. C. J., Hamilton, D. S., Mahowald, N. M., Nagatsuka, N., Ohata, S., Uetake, J., Kondo, Y., and Koike, M.: Glacially sourced dust as a potentially significant source of ice nucleating particles, *Nat. Geosci.*, 12, 253–258, <https://doi.org/10.1038/s41561-019-0314-x>, 2019.
- Tonboe, R., Lavelle, J., Pfeiffer, R.-H., and Howe, E.: Product User Manual for OSI SAF Global Sea Ice Concentration – Product OSI-401-b, Danish Meteorological Institute, Denmark, 2017.
- Turner, D. D.: Arctic Mixed-Phase Cloud Properties from AERI Lidar Observations: Algorithm and Results from SHEBA, *J. Appl. Meteorol.*, 44, 427–444, <https://doi.org/10.1175/JAM2208.1>, 2005.
- Vali, G.: Quantitative Evaluation of Experimental Results on the Heterogeneous Freezing Nucleation of Supercooled Liquids, *J. Atmos. Sci.*, 28, 402–409, [https://doi.org/10.1175/1520-0469\(1971\)028<0402:QEOERA>2.0.CO;2](https://doi.org/10.1175/1520-0469(1971)028<0402:QEOERA>2.0.CO;2), 1971.
- Van Pinxteren, M., Barthel, S., Fomba, K. W., Müller, K., Von Tümpling, W., and Herrmann, H.: The influence of environmental drivers on the enrichment of organic carbon in the sea surface microlayer and in submicron aerosol particles—measurements from the Atlantic Ocean, *Elementa: Science of the Anthropocene*, 5, 35, <https://doi.org/10.1525/elementa.225>, 2017.
- Vavrus, S., Holland, M. M., and Bailey, D. A.: Changes in Arctic clouds during intervals of rapid sea ice loss, *Clim. Dynam.*, 36, 1475–1489, <https://doi.org/10.1007/s00382-010-0816-0>, 2011.
- Welti, A., Müller, K., Fleming, Z. L., and Stratmann, F.: Concentration and variability of ice nuclei in the subtropical maritime boundary layer, *Atmos. Chem. Phys.*, 18, 5307–5320, <https://doi.org/10.5194/acp-18-5307-2018>, 2018.
- Welti, A., Bigg, E. K., DeMott, P. J., Gong, X., Hartmann, M., Harvey, M., Henning, S., Herenz, P., Hill, T. C. J., Hornblow, B., Leck, C., Löffler, M., McCluskey, C. S., Rauker, A. M., Schmale, J., Tatzelt, C., van Pinxteren, M., and Stratmann, F.: Ship-based measurements of ice nuclei concentrations over the Arctic, Atlantic, Pacific and Southern oceans, *Atmos. Chem. Phys.*, 20, 15191–15206, <https://doi.org/10.5194/acp-20-15191-2020>, 2020.
- Wendisch, M., Brückner, M., Burrows, J., Crewell, S., Dethloff, K., Ebell, K., Lüpkes, C., Macke, A., Notholt, J., Quaas, J., Rinke, A., and Tegen, I.: Understanding causes and effects of rapid warming in the Arctic, *Eos*, 98, <https://doi.org/10.1029/2017EO064803>, 2017.
- Wendisch, M., Macke, A., Ehrlich, A., Lüpkes, C., Mech, M., Chechin, D., Dethloff, K., Velasco, C. B., Bozem, H., Brückner, M., Clemen, H.-C., Crewell, S., Donth, T., Dupuy, R., Ebell, K., Egerer, U., Engelmann, R., Engler, C., Eppers, O., Gehrman, M., Gong, X., Gottschalk, M., Gourbeyre, C., Griesche, H., Hartmann, J., Hartmann, M., Heinold, B., Herber, A., Herrmann, H., Heygster, G., Hoor, P., Jafariserajehlou, S., Jäkel, E., Järvinen, E., Jourdan, O., Kästner, U., Kecorius, S., Knudsen, E. M., Köllner, F., Kretschmar, J., Lelli, L., Leroy, D., Maturilli, M., Mei, L., Mertes, S., Mioche, G., Neuber, R., Nicolaus, M., Nomokonova, T., Notholt, J., Palm, M., van Pinxteren, M., Quaas, J., Richter, P., Ruiz-Donoso, E., Schäfer, M., Schmieder, K., Schnaiter, M., Schneider, J., Schwarzenböck, A., Seifert, P., Shupe, M. D., Siebert, H., Spreen, G., Stapf, J., Stratmann, F., Vogl, T., Welti, A., Wex, H., Wiedensohler, A., Zannata, M., and Zeppenfeld, S.: The Arctic Cloud Puzzle: Using ALOUD/PASCAL Multiplatform Observations to Unravel the Role of Clouds and Aerosol Particles in Arctic Amplification, *B. Am. Meteorol. Soc.*, 100, 841–871, <https://doi.org/10.1175/BAMS-D-18-0072.1>, 2019.
- Wex, H., Huang, L., Zhang, W., Hung, H., Traversi, R., Becagli, S., Sheesley, R. J., Moffett, C. E., Barrett, T. E., Bossi, R., Skov, H., Hünerbein, A., Lubitz, J., Löffler, M., Linke, O., Hartmann, M., Herenz, P., and Stratmann, F.: Annual variability of ice-nucleating particle concentrations at different Arctic locations, *Atmos. Chem. Phys.*, 19, 5293–5311, <https://doi.org/10.5194/acp-19-5293-2019>, 2019.
- Wiedensohler, A., Orsini, D., Covert, D. S., Coffmann, D., Cantrell, W., Havlicek, M., Brechtel, F. J., Russell, L. M., Weber, R. J., Gras, J., Hudson, J. G., and Litchy, M.: Intercomparison Study of the Size-Dependent Counting Efficiency of 26 Condensation Particle Counters, *Aerosol Sci. Tech.*, 27, 224–242, <https://doi.org/10.1080/02786829708965469>, 1997.
- Wiedensohler, A., Birmili, W., Nowak, A., Sonntag, A., Weinhold, K., Merkel, M., Wehner, B., Tuch, T., Pfeifer, S., Fiebig, M., Fjåraa, A. M., Asmi, E., Sellegri, K., Depuy, R., Venzac, H., Villani, P., Laj, P., Aalto, P., Ogren, J. A., Swietlicki, E., Williams, P., Roldin, P., Quincey, P., Hüglin, C., Fierz-Schmidhauser, R., Gysel, M., Weingartner, E., Riccobono, F., Santos, S., Grünig, C., Faloon, K., Beddows, D., Harrison, R., Monahan, C., Jennings, S. G., O'Dowd, C. D., Marinoni, A., Horn, H.-G., Keck, L., Jiang, J., Scheckman, J., McMurry, P. H., Deng, Z., Zhao, C. S., Moerman, M., Henzing, B., de Leeuw, G., Löschau, G., and Bastian, S.: Mobility particle size spectrometers: harmonization of technical standards and data structure to facilitate high quality long-term observations of atmospheric particle number size distributions, *Atmos. Meas. Tech.*, 5, 657–685, <https://doi.org/10.5194/amt-5-657-2012>, 2012.
- Wiedensohler, A., Wiesner, A., Weinhold, K., Birmili, W., Herrmann, M., Merkel, M., Müller, T., Pfeifer, S., Schmidt, A., Tuch, T., Velarde, F., Quincey, P., Seeger, S., and Nowak, A.: Mobility particle size spectrometers: Calibration procedures and measurement uncertainties, *Aerosol Sci. Tech.*, 52, 146–164, <https://doi.org/10.1080/02786826.2017.1387229>, 2018.
- Wilson, T. W., Ladino, L. A., Alpert, P. A., Breckels, M. N., Brooks, I. M., Browse, J., Burrows, S. M., Carslaw, K. S., Huffman, J. A., Judd, C., Kilhau, W. P., Mason, R. H., McFiggans, G., Miller, L. A., Nájera, J. J., Polishchuk, E., Rae, S., Schiller, C. L., Si, M., Temprado, J. V., Whale, T. F., Wong, J. P. S., Wurl, O., Yakobi-Hancock, J. D., Abbatt, J. P., Aller, J. Y., Bertram, A. K., Knopf, D. A., and Murray, B. J.: A marine biogenic source of atmospheric ice-nucleating particles, *Nature*, 525, 234–238, <https://doi.org/10.1038/nature14986>, 2015.
- Xi, Y., Mercier, A., Kuang, C., Yun, J., Christy, A., Melo, L., Maldonado, M. T., Raymond, J. A., and Bertram, A. K.: Concentrations and properties of ice nucleating substances in exudates from

Antarctic sea-ice diatoms, *Environmental Science: Processes & Impacts*, 23, 323–334, <https://doi.org/10.1039/D0EM00398K>, 2021.

Zeppenfeld, S., van Pinxteren, M., Hartmann, M., Bracher, A., Stratmann, F., and Herrmann, H.: Glucose as a potential chemical marker for ice nucleating activity in Arctic seawater and melt pond samples, *Environ. Sci. Technol.*, 53, acs.est.9b01469, <https://doi.org/10.1021/acs.est.9b01469>, 2019.